J. Fluid Mech. (1989), *vol.* 200, *pp.* 235–264
Printed in Great Britain

The complete second-order diffraction solution for an axisymmetric body Part 1. Monochromatic incident waves

By MOO-HYUN KIM AND DICK K. P. YUE
Department of Ocean Engineering, Massachusetts Institute of Technology, Cambridge, MA 02139, USA

(Received 12 April 1988)

We study the diffraction, to second order, of plane monochromatic incident gravity waves by a vertically axisymmetric body. The second-order double-frequency diffraction potential is obtained explicitly. A sequence of one-dimensional integral equations along the generator of the body involving free-surface ring sources of general order are formulated and solved for the circumferential components of the second-order potential. The solution is expedited by analytic integration in the entire local-wave-free outer field of a requisite free-surface integral. The method is validated by extensive convergence tests and comparisons to semi-analytic results for the second-order forces and moments on a uniform vertical circular cylinder. Complete second-order forces, moments, surface pressures and run-up on the vertical cylinder as well as a truncated vertical cone are presented. A summary of the important findings is given in §5.

1. Introduction

When nonlinear effects are included in the diffraction of waves by a body, there are, at second order, interactions at the sums and differences of the component frequencies of the incident waves. Although the magnitudes of these nonlinear effects are in general only second order, they act at frequencies away from that of the ambient wave energy, and may therefore be of primary concern especially when such excitations are near the natural periods of the body motions or where restoring or damping forces are small. In certain other cases, such as for non-wall-sided geometries (see §4), second-order effects may also be an appreciable part of the total excitation and are therefore important corrections to the linearized results.

Despite its importance, theoretical developments of the second-order diffraction problem have until recently (e.g. Ogilvie 1983) been scant. Even for the simple geometry of the uniform vertical circular cylinder, the results were controversial (Issacson 1977; Chakrabarti 1978; Molin 1979; Wehausen 1980; Hunt & Baddour 1981; Chen & Hudspeth 1982; Rahman 1983). The principal difficulties are the correct treatment of the second-order free-surface boundary conditions and a proper specification of the radiation condition for the second-order diffracted waves.

A seminal work was that of Molin (1979), who by decomposing the second-order potential into free and forced terms satisfying respectively homogeneous and inhomogeneous free-surface conditions, obtained consistent radiation conditions for the separate components. These results have also been confirmed recently by Wang (1987) who studied the long-time limit of the initial-value problem. To obtain integrated second-order quantities such as forces, Molin avoided the explicit solution

of the double-frequency second-order potential by introducing a fictitious assisting radiation potential at that frequency. Applying Green's identity, an expression for the second-order force can be obtained in terms of the assisting potential and functions of first-order quantities. The method requires the vanishing of a far-field integral – a weak radiation condition guaranteed by the asymptotic behaviours of the second-order potentials. The same approach was suggested independently by Lighthill (1979), and was in fact used by Faltinsen & Löken (1978) for the two-dimensional problem. Molin's solution has since been extended, for example, by Molin & Marion (1986), who obtained some results for second-order motions; by Löken (1986), who also attempted a solution of the second-order potential; and by Eatock Taylor & Hung (1987), who developed a method for the evaluation of the free-surface integral based on leading asymptotics.

In this paper, we consider the direct solution of the second-order diffraction problem. A Green's theorem integral equation is obtained for the second-order diffraction potential involving the (double-frequency) wave-source Green function. This equation is similar to that for the linear problem with the exception of a forcing term involving products of first-order potentials which is a slowly converging integral over the entire free surface. An effective evaluation of this integral is essential to the solution of the problem and a detailed asymptotic method which performs the integration analytically in the entire local-wave-free outer domain is developed. Since the second-order potential is obtained explicitly, complete second-order local quantities such as pressures, velocities and surface elevations are readily available in addition to integrated forces and moments.

For simplicity, we consider bodies that possess vertical axes of symmetry. Expressing the potentials in terms of Fourier series in the circumferential coordinate, we obtain after integration a sequence of one-dimensional integral equations along the generator of the body for each Fourier component with free-surface ring-source kernels of the corresponding order. For linear problems involving axisymmetric bodies, the ring-source distribution method was used by Black (1975), and later by Fenton (1978) and Hulme (1983), who gave particular attention to the treatment of singularities and the convergence of representations of the ring source and its derivatives. Their numerical examples are, however, limited to the first two Fourier modes. For the diffraction problem, we present here an analysis and numerical method for the arbitrary-order ring-source potential and its gradient.

To illustrate the present method, we present computational results for a uniform vertical circular cylinder and for a truncated conical body, both in finite depth. The validity and accuracy of the method is demonstrated by extensive results for convergence with respect to body discretizations, number of circumferential modes, and free-surface integral evaluation, as well as comparisons to semianalytic solutions for the second-order forces and moments for the vertical cylinder derived in Appendix B. Detailed results for the linear and second-order mean and double-frequency forces, moments, pressure distributions and run-up on the bodies are presented and discussed in §4. Important features of second-order diffraction effects are summarized in §5.

We have studied the diffraction by a single monochromatic wave. The solution of sum- and difference-frequency second-order diffraction in the presence of bichromatic incident waves as well as the radiation problem are considered in a forthcoming paper, Part 2. Many of the techniques developed here can be extended to general three-dimensional bodies, and an outline is presented in the conclusion section.

2. Formulation of the second-order problem

2.1. *The boundary-value problem*

We consider the linear and second-order diffraction of a plane monochromatic incident wave, frequency ω, linear amplitude A, by a fixed three-dimensional body in constant water depth, h. Cartesian coordinates with the (x, y)-plane in the quiescent free surface and z positive upward are chosen. Assuming potential flow and weakly nonlinear waves, we express the total velocity potential Φ as a perturbation series in the wave-slope parameter, $\epsilon \equiv kA \ll 1$:

$$\Phi = \epsilon \Phi^{(1)} + \epsilon^2 \Phi^{(2)} + \dots, \tag{2.1}$$

where k is the incident wavenumber given by the dispersion relationship $\omega^2 = gk \tanh(kh)$, g being the gravitational acceleration. For monochromatic incident waves, we separate the time dependencies explicitly and write

$$\left.\begin{aligned} \Phi^{(1)}(x, y, z, t) &= \mathrm{Re}\{\phi^{(1)}(x, y, z)\, \mathrm{e}^{-\mathrm{i}\omega t}\}, \\ \Phi^{(2)}(x, y, z, t) &= \mathrm{Re}\{\phi^{(2)}(x, y, z)\, \mathrm{e}^{-2\mathrm{i}\omega t}\} + \bar{\Phi}^{(2)}(x, y, z). \end{aligned}\right\} \tag{2.2}$$

Note that the contribution of the steady part of the second-order potential in (2.2) to the pressure (hence forces) or free-surface elevation is at most $O(\epsilon^3)$. At each order, the boundary-value problem is linear and we decompose ϕ into incident (ϕ_I) and diffracted (ϕ_D) potentials: $\phi^{(i)} = \phi_\mathrm{I}^{(i)} + \phi_\mathrm{D}^{(i)}$, $i = 1, 2$. The incidence potentials are given from Stokes' waves:

$$\phi_\mathrm{I}^{(1)} = \frac{-\mathrm{i}gA}{\omega} \frac{\cosh k(z+h)}{\cosh kh} \mathrm{e}^{\mathrm{i}kx}, \tag{2.3a}$$

$$\phi_\mathrm{I}^{(2)} = \frac{-3\mathrm{i}\omega A^2}{8} \frac{\cosh 2k(z+h)}{\sinh^4 kh} \mathrm{e}^{\mathrm{i}2kx}, \tag{2.3b}$$

for a wave incident from $x \sim -\infty$. The boundary-value problems governing the first- and second-order diffraction potentials are respectively

$$\nabla^2 \phi_\mathrm{D}^{(1)} = 0 \qquad \text{in the fluid } (z < 0); \tag{2.4a}$$

$$\left(-\omega^2 + g\frac{\partial}{\partial z}\right)\phi_\mathrm{D}^{(1)} = 0 \qquad \text{on } z = 0\ (S_\mathrm{F}); \tag{2.4b}$$

$$\frac{\partial \phi_\mathrm{D}^{(1)}}{\partial z} = 0 \qquad \text{on } z = -h; \tag{2.4c}$$

$$\frac{\partial \phi_\mathrm{D}^{(1)}}{\partial n} = -\frac{\partial \phi_\mathrm{I}^{(1)}}{\partial n} \qquad \text{on the body } (S_\mathrm{B}); \tag{2.4d}$$

$$\lim_{k\rho \to \infty} \rho^{\frac{1}{2}}\left(\frac{\partial}{\partial \rho} - \mathrm{i}k\right)\phi_\mathrm{D}^{(1)} = 0, \qquad k\rho \gg 1\ (S_\infty); \tag{2.4e}$$

and

$$\nabla^2 \phi_\mathrm{D}^{(2)} = 0 \qquad \text{in the fluid } (z < 0); \tag{2.5a}$$

$$\left(-4\omega^2 + g\frac{\partial}{\partial z}\right)\phi_\mathrm{D}^{(2)} = q \qquad \text{on } z = 0\ (S_\mathrm{F}); \tag{2.5b}$$

$$\frac{\partial \phi_\mathrm{D}^{(2)}}{\partial z} = 0 \qquad \text{on } z = -h; \tag{2.5c}$$

$$\frac{\partial \phi_\mathrm{D}^{(2)}}{\partial n} = -\frac{\partial \phi_\mathrm{I}^{(2)}}{\partial n} \qquad \text{on the body } (S_\mathrm{B}); \tag{2.5d}$$

plus a suitable radiation condition at infinity. In the above $\rho \equiv (x^2+y^2)^{\frac{1}{2}}$ is the radial distance from the origin, and $\partial/\partial n$ the normal derivative into the body. The first-order problem (2.4) is classical, and a variety of numerical methods are now available (e.g. Mei 1978).

The second-order problem is complicated by the inhomogeneous forcing term in the free-surface boundary condition (2.5*b*), which is given in terms of quadratic products of the first-order potential:

$$q = \left[-\frac{\mathrm{i}\omega}{2g}\phi^{(1)}\left(-\omega^2\frac{\partial\phi^{(1)}}{\partial z} + g\frac{\partial^2\phi^{(1)}}{\partial z^2}\right) + \mathrm{i}\omega\,(\nabla\phi^{(1)})^2 \right]_{z=0} - q_{\mathrm{II}}, \tag{2.6}$$

where the contribution from quadratic products of the incident potential $\phi_{\mathrm{I}}^{(1)}$ itself, q_{II}, is subtracted out owing to the free-surface condition satisfied by (2.3*b*). The specific radiation condition for $\phi_{\mathrm{D}}^{(2)}$ depends on the far-field behaviour of q. In general, if the free-surface forcing is absolutely integrable, the validity of a Sommerfeld-like radiation condition (2.4*e*) follows directly from Cauchy–Poisson theory (Stoker 1957). In the present case, q contains quadratic products of $\phi_{\mathrm{D}}^{(1)}$ itself (q_{DD}), as well as products of $\phi_{\mathrm{D}}^{(1)}$ and a non-diminishing $\phi_{\mathrm{I}}^{(1)}$ (q_{ID}), and a more careful asymptotic analysis is necessary. From (2.4*e*), q_{DD} decays as $O(1/\rho)$ for $\rho \gg 1$, while the far-field asymptotic of q_{ID} is

$$q_{\mathrm{ID}} \sim \rho^{-\frac{1}{2}}\mathrm{e}^{\mathrm{i}k\rho(1+\cos\theta)} + O(\rho^{-\frac{3}{2}}), \quad \rho \gg 1. \tag{2.7}$$

Following Molin (1979), we decompose $\phi_{\mathrm{D}}^{(2)}$ into a homogeneous (free waves), ϕ_{H}, and a particular (locked waves) solution, ϕ_{P}, which satisfy respectively the homogeneous and inhomogeneous free-surface conditions (2.5*b*), and jointly the inhomogeneous body boundary condition (2.5*d*). The boundary-value problem for ϕ_{H} is similar to (2.4) and its far-field behaviour is given by

$$\phi_{\mathrm{H}} \sim \rho^{-\frac{1}{2}}\mathrm{e}^{\mathrm{i}k_2\rho} + O(\rho^{-\frac{3}{2}}), \quad \rho \gg 1, \tag{2.8}$$

where k_2 is the double-frequency wavenumber satisfying $4\omega^2 = k_2 g \tanh(k_2 h)$. From (2.7), ϕ_{P} has the asymptotic form

$$\phi_{\mathrm{P}} \sim \rho^{-\frac{1}{2}}P(\theta,z)\,\mathrm{e}^{\mathrm{i}k\rho(1+\cos\theta)} + O(1/\rho), \quad \rho \gg 1, \tag{2.9}$$

where, satisfying the bottom condition, and the field equation to leading order, $P(\theta,z)$ is given by

$$P(\theta,z) = p(\theta)\cosh\{k\,[2(1+\cos\theta)]^{\frac{1}{2}}(z+h)\} + O(\rho^{-\frac{1}{2}}). \tag{2.10}$$

Note that this 'forced' second-order potential does not attenuate with depth on the weather-side ray, $\theta = \pi$, far away from the body. The asymptotic forms (2.8), (2.9) for the free and locked wave potentials were first obtained by Molin (1979) and subsequently confirmed by the analysis of Wang (1987) who considered the long-time limit of the initial-value problem.

2.2. *The boundary-integral equation for the second-order potential*

We introduce the linear wave-source Green function at double-frequency (2ω), $G^+(\boldsymbol{x},\boldsymbol{x}')$, where $\boldsymbol{x}$, $\boldsymbol{x}'$ represent respectively the field and source points. Applying Green's second identity to $\phi_{\mathrm{D}}^{(2)}$ and G^+, and using (2.5) and the boundary conditions satisfied by G^+, we obtain for $\boldsymbol{x}' \in S_{\mathrm{B}}$ a second-kind Fredholm integral equation for $\phi_{\mathrm{D}}^{(2)}$:

$$2\pi\,\phi_{\mathrm{D}}^{(2)}(\boldsymbol{x}') + \iint_{S_{\mathrm{B}}} \phi_D^{(2)}\frac{\partial G^+}{\partial n}\,\mathrm{d}\boldsymbol{x} = -\iint_{S_{\mathrm{B}}} G^+\frac{\partial\phi_{\mathrm{I}}^{(2)}}{\partial n}\,\mathrm{d}\boldsymbol{x} + \frac{1}{g}\iint_{S_{\mathrm{F}}} qG^+\,\mathrm{d}\boldsymbol{x}, \tag{2.11}$$

where the integral over the far-field vanishes as $\rho \to \infty$:

$$\iint_{S_\infty} \left(\frac{\partial \phi_{\mathrm{D}}^{(2)}}{\partial n} G^+ - \phi_{\mathrm{D}}^{(2)} \frac{\partial G^+}{\partial n} \right) \mathrm{d}\boldsymbol{x} = 0, \tag{2.12}$$

upon using the method of stationary phase in conjunction with the asymptotic results (2.8), (2.9). From the point of view of the integral equation (2.11) (not considering irregular frequencies associated with S_{B}), the 'weak' radiation condition (2.12) is sufficient for the uniqueness of the diffraction problem (Finkelstein 1957; Peters & Stoker 1957). Interestingly, it can be shown that (2.12) holds for the diffraction potentials at all orders.

The integral equation (2.11) is identical in form to that for a linear diffraction problem with the exception of the free-surface integral which extends to infinity. From the far-field behaviours of q and G^+, the integrand diminishes only as ρ^{-1} for $\rho \gg 1$, and is highly oscillatory, being the product of three wave-like functions. An accurate and efficient evaluation of this slowly converging forcing term is essential to the solution of (2.11) and a procedure involving analytic integrations in the local-wave-free domain is developed in §2.4.

For bodies that are vertically axisymmetric about $\rho = 0$, the integral equation (2.11) over a surface can be reduced to a sequence of boundary-integral problems over a line in the (ρ, z)-plane. To accomplish this, we expand $\phi_{\mathrm{I}}^{(2)}$, $\phi_{\mathrm{D}}^{(2)}$, q and G^+ into Fourier-cosine series in the circumferential coordinate θ:

$$\left.\begin{aligned} \begin{Bmatrix} \phi_{\mathrm{I,D}}^{(2)}(\rho,\theta,z) \\ q(\rho,\theta) \end{Bmatrix} &= \sum_{n=0}^{\infty} \begin{Bmatrix} \phi_{\mathrm{I,D}n}^{(2)}(\rho,z) \\ q_n(\rho) \end{Bmatrix} \cos n\theta, \\ G^+(\rho,\theta,z;\rho',\theta',z') &= \sum_{n=0}^{\infty} \frac{\epsilon_n}{2\pi} G_n^+(\rho,z;\rho',z') \cos n(\theta-\theta'), \end{aligned}\right\} \tag{2.13}$$

where $\epsilon_0 = 1$, $\epsilon_n = 2$ for $n \geqslant 1$. Substituting (2.13) into (2.11), performing the integration in θ and equating Fourier coefficients in θ', we obtain a one-dimensional integral equations for each Fourier mode, $\phi_{\mathrm{D}n}^{(2)}$:

$$2\pi \phi_{\mathrm{D}n}^{(2)} + \oint_{\partial B} \mathrm{d}l\, \rho\, \phi_{\mathrm{D}n}^{(2)} \frac{\partial G_n^+}{\partial n} = -\int_{\partial B} \mathrm{d}l\, \rho \frac{\partial \phi_{\mathrm{I}n}^{(2)}}{\partial n} G_n^+ + \frac{1}{g} \int_{\partial F} \mathrm{d}\rho\, \rho q_n\, G_n^+, \tag{2.14}$$

where the line integrals are along the traces ∂B, ∂F of S_{B} and S_{F} respectively on (ρ, z). In the above, the nth mode of the inhomogeneous free-surface forcing term, q_n, can be obtained from (2.6):

$$\left.\begin{aligned} q_0 &= \frac{\mathrm{i}\omega}{2} \sum_{m=0}^{\infty} \frac{1}{\epsilon_m} \left\{ \left(\nu \frac{\partial \phi_m^{(1)}}{\partial z} - \frac{\partial^2 \phi_m^{(1)}}{\partial z^2} \right) \phi_m^{(1)} + 2 \left[\left(\frac{\partial \phi_m^{(1)}}{\partial \rho} \right)^2 + \left(\frac{\partial \phi_m^{(1)}}{\partial z} \right)^2 \right] + \frac{m^2 \epsilon_m}{\rho^2} \phi_m^{(1)2} \right\} - q_{\mathrm{II}0}, \\ q_n &= \frac{\mathrm{i}\omega}{2} \sum_{m=0}^{n} \left\{ \frac{1}{2} \left(\nu \frac{\partial \phi_{n-m}^{(1)}}{\partial z} - \frac{\partial^2 \phi_{n-m}^{(1)}}{\partial z^2} \right) \phi_m^{(1)} + \frac{\partial \phi_{n-m}^{(1)}}{\partial \rho} \frac{\partial \phi_m^{(1)}}{\partial \rho} + \frac{\partial \phi_{n-m}^{(1)}}{\partial z} \frac{\partial \phi_m^{(1)}}{\partial z} - \frac{(n-m)\, m}{\rho^2} \phi_{n-m}^{(1)} \phi_m^{(1)} \right\} \\ &\quad + \frac{\mathrm{i}\omega}{2} \sum_{m=0}^{\infty} \left\{ \frac{1}{2} \left(\nu \frac{\partial \phi_m^{(1)}}{\partial z} - \frac{\partial^2 \phi_m^{(1)}}{\partial z^2} \right) \phi_{n+m}^{(1)} + \frac{1}{2} \left(\nu \frac{\partial \phi_{n+m}^{(1)}}{\partial z} - \frac{\partial^2 \phi_{n+m}^{(1)}}{\partial z^2} \right) \phi_m^{(1)} \right. \\ &\quad \left. + 2 \left(\frac{\partial \phi_m^{(1)}}{\partial \rho} \frac{\partial \phi_{n+m}^{[1]}}{\partial \rho} + \frac{\partial \phi_m^{(1)}}{\partial z} \frac{\partial \phi_{n+m}^{(1)}}{\partial z} \right) + \frac{2m(n+m)}{\rho^2} \phi_m^{(1)} \phi_{n+m}^{(1)} \right\} - q_{\mathrm{II}n}, \quad n = 1, 2, \ldots, \end{aligned}\right\} \tag{2.15}$$

where $\nu \equiv \omega^2/g, \phi_m^{(1)}$ is the mth Fourier coefficient of $\phi^{(1)}$, and all quantities are evaluated on $z = 0$. Noting that $G^+(\rho, \theta, z; \rho', \theta', z') = G^+(\rho, z; \rho', z'; \cos(\theta - \theta'))$, the nth mode ring source defined in (2.13) can also be expressed as

$$G_n^+(\rho, z; \rho', z') = \int_0^{2\pi} G^+(\rho, z; \rho', z'; \cos(\theta - \theta')) \cos n(\theta - \theta') \, \mathrm{d}(\theta - \theta'). \tag{2.16}$$

2.3. *Evaluation of the general-order ring-source potential and its derivatives*

The ring-source potential and its normal derivative in (2.14) have been analysed by a number of investigators (Fenton 1978; Hulme 1983; Fernandes 1983) although numerical results have usually been restricted to the zeroth and first mode only. In order to solve for the diffraction potential itself, we develop here a computational algorithm for the general-order problem.

The wave-source Green function $G(\boldsymbol{x}; \boldsymbol{x}')$ can be expressed as a sum of its Rankine source and image, and a regular part:

$$G = \frac{1}{r} + \frac{1}{r'} + W, \tag{2.17}$$

where $r^2 \equiv R^2 + (z - z')^2$, $r'^2 \equiv R^2 + (z + z')^2$, and $R^2 \equiv \rho^2 + \rho'^2 - 2\rho\rho' \cos(\theta - \theta')$.

For the $1/r$ Rankine part of (2.17) (the analysis for $1/r'$ is analogous), the circumferential integration (2.16) can be obtained analytically for any n in terms of second-kind Legendre functions of integral-minus-half order (Abramowitz & Stegun 1964):

$$R_n \equiv \int_0^{2\pi} \frac{\cos n(\theta - \theta')}{r} \mathrm{d}(\theta - \theta') = \frac{2}{(\rho\rho')^{\frac{1}{2}}} Q_{n-\frac{1}{2}}(a_0/b_0), \quad n = 0, 1, 2, \ldots, \tag{2.18}$$

where $a_0 \equiv \rho^2 + \rho'^2 + (z - z')^2$ and $b_0 \equiv 2\rho\rho'$. For the first two modes, $n = 0, 1$, (2.18) can be evaluated directly in terms of complete elliptic integrals of the first and second kind (K and E respectively):

$$\left.\begin{aligned} R_0 &= 2(X/\rho\rho')^{\frac{1}{2}} K(X), \\ R_1 &= 2(\rho\rho')^{-\frac{1}{2}} [Z X^{\frac{1}{2}} K(X) - 2X^{-\frac{1}{2}} E(X)], \end{aligned}\right\} \tag{2.19}$$

where $X \equiv 2b_0/(a_0 + b_0)$ and $Z \equiv a_0/b_0$.

For the higher modes, evaluations using the forward recurrence relationship for $Q_{n-\frac{1}{2}}$ starting from (2.19) are unstable. Thus for $n \geqslant 2$, we utilize instead the hypergeometric function representation of Q:

$$Q_{n-\frac{1}{2}}(Z) = \frac{\pi^{\frac{1}{2}}}{(2Z)^{n+\frac{1}{2}}} \frac{\Gamma(n + \frac{1}{2})}{\Gamma(n+1)} F\left(\tfrac{1}{2}n + \tfrac{3}{4}, \tfrac{1}{2}n + \tfrac{1}{4}, n+1, \frac{1}{Z^2}\right), \tag{2.20}$$

where Γ and F are respectively gamma and hypergeometric functions, and $Z > 1$ in (2.20). If the field point is not close to the ring source, the hypergeometric series representation,

$$F = \frac{\Gamma(n+1)}{\Gamma(\frac{1}{2}n + \frac{3}{4}) \Gamma(\frac{1}{2}n + \frac{1}{4})} \sum_{m=0}^{\infty} \frac{\Gamma(m + \frac{1}{2}n + \frac{3}{4}) \Gamma(m + \frac{1}{2}n + \frac{1}{4})}{\Gamma(m + n + 1) \Gamma(m + 1)} \frac{1}{Z^{2m}}, \tag{2.21}$$

converges rapidly, and (2.20) can be evaluated accordingly. As the field point approaches the ring source, i.e. as $Z \to 1+$, the logarithmic singularity can be excluded explicitly:

$$F = \frac{\Gamma(n+1)}{\Gamma(\frac{1}{2}n+\frac{3}{4})\,\Gamma(\frac{1}{2}n+\frac{1}{4})} \sum_{m=0}^{\infty} \frac{(\frac{1}{2}n+\frac{3}{4})_m\,(\frac{1}{2}n+\frac{1}{4})_m}{\Gamma(m+1)^2}$$

$$\times \left[2\Psi(m+1) - \Psi(\tfrac{1}{2}n+\tfrac{3}{4}+m) - \Psi(\tfrac{1}{2}n+\tfrac{1}{4}+m) - \ln\left(1-\frac{1}{Z^2}\right)\right]\left(1-\frac{1}{Z^2}\right)^m, \quad (2.22)$$

where Ψ is Euler's psi function and $(x)_m \equiv \Gamma(x+m)/\Gamma(x)$; and (2.22) is useful for $Z-1 \ll 1$.

The singularity of the n-mode ring source near the source ring is given by the asymptotic behaviour of $Q_{n-\frac{1}{2}}$ as $Z \to 1$, which can be inferred from (2.22) for $m = 0$:

$$Q_{n-\frac{1}{2}}(Z) \sim -\tfrac{1}{2}\ln\left(1-\frac{1}{Z^2}\right) + \Psi(1) - \Psi(n+\tfrac{1}{2}) + \ln 2, \quad Z \to 1. \quad (2.23)$$

The corresponding behaviour for R_n is

$$R_n \sim \frac{2}{\rho'}\{-\tfrac{1}{2}\ln[(\rho-\rho')^2+(z-z')^2] + \ln\rho + 3\ln 2 - c_n\}, \quad (2.24)$$

where c_n are constants given by $c_0 = 0$, and

$$c_n = 2\left[1+\frac{1}{3}+\frac{1}{5}+\ldots+\frac{1}{2n-1}\right] \quad \text{for } n \geqslant 1.$$

It is of interest to note that the logarithmic singularity of R_n is the same for all n. For computations, the two complementary expressions (2.21), (2.22) for the hypergeometric functions are first converted to economized Chebyshev polynomials for a specific equal-ripple error in the whole domain $Z > 1$ (Luke 1975).

The nth-mode Rankine kernel of the integral equation (2.14) can be obtained in a similar manner:

$$\begin{aligned}\frac{\partial}{\partial n}R_n &= \left(n_\rho\frac{\partial}{\partial\rho}+n_z\frac{\partial}{\partial z}\right)R_n \\ &= -\frac{n_\rho}{\rho(\rho\rho')^{\frac{1}{2}}}\left\{Q_{n-\frac{1}{2}}(Z)+\frac{2n-1}{a_0+b_0}[a_0 Q_{n-\frac{1}{2}}(Z)-b_0 Q_{n-\frac{3}{2}}(Z)]\right\} \\ &\quad + \frac{2}{(\rho\rho')^{\frac{1}{2}}}\frac{2n-1}{a_0^2-b_0^2}[(\rho-\rho')\,n_\rho+(z-z')\,n_z]\,[a_0 Q_{n-\frac{1}{2}}(Z)-b_0 Q_{n-\frac{3}{2}}(Z)], \quad (2.25)\end{aligned}$$

where n_ρ and n_z are respectively the components of the unit normal vector $\boldsymbol{n}$ in the ρ- and z-directions. The apparent Cauchy singularity in the last term of (2.25) vanishes identically when the source point approaches the interior of piecewise linear segments approximating the body boundary ∂B, and is otherwise finite for a body contour with continuous slope.

The behaviour of (2.25) as the field point approaches the source ring is given by

$$\frac{\partial R_n}{\partial n} \sim \frac{-n_\rho}{\rho\rho'}\{-\tfrac{1}{2}\ln[(\rho-\rho')^2+(z-z')^2] + \ln\rho + 3\ln 2 - d_n\}, \quad (2.26)$$

where d_n are constants given in terms of $c_n : d_0 = 1$, and

$$d_n = (n+\tfrac{1}{2})\,c_n - (n-\tfrac{1}{2})\,c_{n-1}, \quad n \geqslant 1. \tag{2.27}$$

As before, the logarithmic singularity is identical for all n.

For the non-singular part of the Green function (2.17), the nth-mode ring source, W_n, is simply the Fourier-series coefficient of W:

$$W_n(\rho, z; \rho', z') = \int_0^{2\pi} W(\rho, z; \rho', z'; \cos(\theta-\theta'))\cos n(\theta-\theta')\,\mathrm{d}(\theta-\theta'), \quad n \geqslant 0. \tag{2.28}$$

Since W is periodic in $(\theta-\theta')$, the convergence of W_n with n is a function only of the smoothness of W. For computations, we truncate the number of modes at $n = N$, and the W_n are given by discrete inverse Fourier transform:

$$W_n = \frac{4\pi}{\epsilon_n \epsilon_n' N} \sum_{m=0}^{N} \frac{1}{\epsilon_m'} \cos\left(\frac{nm\pi}{N}\right) W\left(\cos\left(\frac{m\pi}{N}\right)\right), \quad n = 0, 1, \ldots, N, \tag{2.29}$$

where $\epsilon_n' \equiv 2$ for $n = 0, N$, and $\epsilon_n' \equiv 1$ for $n = 1, 2, \ldots, N-1$. Thus, only $N+1$ evaluations of the Green function W are required to evaluate the $N+1$ modes of the regular ring source W_n, and the error is measured by the last term W_N. In practice, the convergence of W_n with n may be slower than that of the potentials so that more evaluations, say $N_W > N$, are used for the W_n, $n = 0, 1, \ldots, N$. Efficient algorithms for the evaluation of W are now available (e.g. Newman 1985) and are not detailed here.

We now turn to the far-field behaviour of the general-order ring source. For $R/h \gg 1$, a useful expression for G is (John 1950)

$$G = -2\pi i C_0 \cosh k(z+h) \cosh k(z'+h)\, H_0(kR) + 4 \sum_{m=1}^{\infty} C_m \cos \kappa_m(z+h) \cos \kappa_m(z'+h)\, K_0(\kappa_m R), \tag{2.30}$$

where H_0, K_0 are the zeroth-order first-kind Hankel function and second-kind modified Bessel function,

$$C_0 = \frac{\nu^2 - k^2}{k^2 h - \nu^2 h + \nu}, \quad C_m = \frac{\kappa_m^2 + \nu^2}{\kappa_m^2 h + \nu^2 h - \nu}, \tag{2.31}$$

and κ_m, $m = 1, 2, \ldots$, are the real roots of the equation

$$\omega^2 = -\kappa_m g \tan \kappa_m h, \quad (m-\tfrac{1}{2})\,\pi \leqslant \kappa_m h \leqslant m\pi. \tag{2.32}$$

For finite depth, the second term in (2.30) is local (evanescent) modes which decay exponentially with radial distance, $\kappa_m R$, and the far-field asymptotic of G is given by the first term which represents outgoing waves:

$$G = -2\pi i C_0 \cosh k(z+h) \cosh k(z'+h)\, H_0(kR) + O(\mathrm{e}^{-\kappa_1 R}). \tag{2.33}$$

The far-field asymptotic of the ring sources, upon using the addition theorem, is

$$G_n = -4\pi^2 i C_0 \cosh k(z+h) \cosh k(z'+h)\, J_n(k\rho')\, H_n(k\rho) + O(\mathrm{e}^{-\kappa_1 R}). \tag{2.34}$$

We remark that as depth increases, the rate of exponential decay of the local modes decreases according to (2.32), and is only algebraic ($\sim R^{-2}$) for infinitely deep water (Newman 1967):

$$G = 2\pi i\nu\, e^{\nu(z+z')} H_0(\nu R) + O(R^{-2}). \tag{2.35}$$

2.4. *Evaluation of the free-surface integral in (2.14)*

The most difficult and computationally expensive aspect of the solution of the integral equations (2.14) is the efficient and accurate evaluation of the free-surface integrals:

$$I_n(\rho', z') \equiv \frac{1}{g}\int_a^\infty d\rho\, \rho q_n(\rho)\, G_n^+(\rho, 0, ; \rho', z'), \tag{2.36}$$

where a is the radius of the waterplane. The forcing terms, q_n, are given in (2.15) in terms of first-order potentials, which may in turn be obtained through an integral equation of the form (2.14) (minus the free-surface integral). We use instead a source-distribution representation for the first-order potential:

$$\phi_{Dn}^{(1)}(\boldsymbol{x}) = \int_{\partial B} dl'\, \rho' \sigma_n(\boldsymbol{x}')\, G_n(\boldsymbol{x}; \boldsymbol{x}'), \tag{2.37}$$

where the ring-source strengths, σ_n, satisfy the second-kind Fredholm integral equation:

$$2\pi\sigma_n(\boldsymbol{x}) + \int_{\partial B} dl'\, \rho' \sigma_n(\boldsymbol{x}') \frac{\partial G_n}{\partial n} = -\frac{\partial \phi_{In}^{(1)}(\boldsymbol{x})}{\partial n}, \quad n = 0, 1, \ldots. \tag{2.38}$$

Equation (2.37) is preferred over a mixed-distribution in evaluating (2.15) since it reduces by one the order of derivatives of the Green function required. Equation (2.38) is solved numerically following a standard procedure of discretizing ∂B into linear segments, assuming a constant source strength over each panel, and selecting collocation points at the mid-points of the segments. The details are omitted. The derivatives of the potential in (2.15) are evaluated by successive differentiation of (2.37).

The free-surface integral, (2.36), is evaluated over two intervals, (a, b) and (b, ∞), where the radius b is chosen so that the latter interval is evanescent-wave free:

$$I_n = \frac{1}{g}\left[\int_a^b d\rho\, \rho q_n G_n^+ + \int_b^\infty d\rho\, \rho \hat{q}_n \hat{G}_n^+ + \int_b^\infty d\rho\, \rho (q_n G_n^+ - \hat{q}_n \hat{G}_n^+)\right]. \tag{2.39}$$

In the above, ($\hat{}$) represents terms that contain contributions from propagating waves only. In our computations, the near-field integral in (2.39) over the finite interval (a, b) is computed by numerical quadrature (Romberg integration) with controlled tolerance. The last integral is made negligibly small by a suitable choice of the partition radius b according to (2.34).

We evaluate the second integral, which is over an infinite domain, analytically. The integrand consists of products of three propagating waves and has a decay rate of $\rho^{-\frac{1}{2}}$ for $\rho \gg 1$. The local-wave-free first-order potential is given by

$$\hat{\phi}_{Dn}^{(1)} = -4\pi^2 i C_0 \cosh k(z+h)\, H_n(k\rho) \int_{\partial B} dl'\, \rho' \sigma_n(\boldsymbol{x}')\, J_n(k\rho') \cosh k(z'+h), \tag{2.40}$$

where the integral over ∂B is simply the nth-mode Kochin function which we denote as L_n. Substituting (2.40) into (2.15), we obtain

$$\left.\begin{aligned}
\hat{q}_0 &= \frac{-\mathrm{i}k^2 g^2 A^2 \cosh^2 kh}{2\omega} \sum_{m=0}^{\infty} \frac{2}{\epsilon_m}\left[\left(\tfrac{3}{2}\tanh^2 kh - \tfrac{1}{2} + \frac{\epsilon_m m^2}{2(k\rho)^2}\right) S_{m,m}(k\rho) + T_{m,m}(k\rho)\right], \\
\hat{q}_n &= \frac{-\mathrm{i}k^2 g^2 A^2 \cosh^2 kh}{2\omega}\left\{\sum_{m=0}^{n}\left[\left(\tfrac{3}{2}\tanh^2 kh - \tfrac{1}{2} - \frac{(n-m)\,m}{(k\rho)^2}\right) S_{n-m,m}(k\rho) + T_{n-m,m}(k\rho)\right]\right. \\
&\quad \left. + 2\sum_{m=0}^{\infty}\left[\left(\tfrac{3}{2}\tanh^2 kh - \tfrac{1}{2} + \frac{(n+m)\,m}{(k\rho)^2}\right) S_{n+m,m}(k\rho) + T_{n+m,m}(k\rho)\right]\right\}, \quad n = 1, 2, \ldots,
\end{aligned}\right\}$$

where

$$\left.\begin{aligned}
S_{m,n}(k\rho) &\equiv \alpha_m \alpha_n H_m(k\rho) H_n(k\rho) + \beta_m \alpha_n J_m(k\rho) H_n(k\rho) + \alpha_m \beta_n H_m(k\rho) J_n(k\rho), \\
T_{m,n}(k\rho) &\equiv \alpha_m \alpha_n H'_m(k\rho) H'_n(k\rho) + \beta_m \alpha_n J'_m(k\rho) H'_n(k\rho) + \alpha_m \beta_n H'_m(k\rho) J'_n(k\rho),
\end{aligned}\right\} \tag{2.41}$$

and primes denote derivatives with respect to argument. The coefficients α_n, β_n, are given by $\alpha_n \equiv -4\pi^2 \mathrm{i} C_0 L_n$, and $\beta_n \equiv \epsilon_n \mathrm{i}^n / \cosh(kh)$. Using (2.34) for G_n, we obtain an expression for the local-wave-free integrand, $\rho \hat{q}_n \hat{G}_n$, of the free-surface integral consisting of triple products of Bessel and Hankel functions multiplied by powers of $k\rho$. The final outer-field integral can be expressed in terms of definite integrals of the forms

$$I^s_{lmn}(kb) = \int_{kb}^{\infty} (k\rho)^s H_l(k\rho)\begin{bmatrix} H^*_m(k\rho) \\ H_m(k\rho) \end{bmatrix} H_n(k_2\rho)\,\mathrm{d}(k\rho), \quad s = 0, \pm 1; \quad l, m, n = 0, 1, \ldots, \tag{2.42}$$

where $(\,)^*$ denotes complex conjugate. A method for the evaluation of these integrals is outlined in Appendix A.

We remark that the exact evaluation of the local-wave-free integral above is critical to the efficacy of the present method. Substituting (2.40) into (2.15), combining with (2.34), and using the leading asymptotics of J_n and H_n for large arguments, it is easy to show that the free-surface integrand has the leading behaviour

$$k\rho G^+_n q_n \sim [\exp(\mathrm{i}(2k + k_2)\rho) + \exp(\mathrm{i}k_2\rho)](k_2\rho)^{-\frac{1}{2}} \quad \text{for} \quad k\rho, k_2\rho \gg 1.$$

Thus if the free-surface integral is simply truncated at b (e.g. Löken 1986), the truncation error decreases only as $b^{-\frac{1}{2}}$. For accurate results, the effort involved in numerical quadrature over a large domain becomes prohibitive. On the other hand, the convergence can be improved by evaluating the integral of the leading asymptotic term only from b to infinity in terms of Fresnel integrals (Eatock Taylor & Hung 1987). The neglected terms are then of $O[\rho^{-\frac{3}{2}}(k^{-1}k_2^{-\frac{1}{2}} + k_2^{-1}k^{-\frac{1}{2}})]$, so that the convergence with b is still only algebraic, in contrast to the exponential decrease of error with b associated only with the evanescent modes in the present case.

3. Second-order exciting forces, moments and surface elevation

The boundary-integral equation (2.14) for $\phi_{Dn}^{(2)}$ is solved using a discretization procedure similar to that for the first-order problem. The hydrodynamic pressure can be calculated from the first- and second-order potentials according to the Bernoulli equation:

$$\frac{-p^{(1)}(t)}{\rho_0} = \frac{\partial \Phi^{(1)}}{\partial t}, \qquad \frac{-p^{(2)}(t)}{\rho_0} = \frac{\partial \Phi^{(2)}}{\partial t} + \tfrac{1}{2}(\nabla \Phi^{(1)})^2, \tag{3.1}$$

where ρ_0 denotes the fluid density. The second-order forces and moments, $f_j^{(2)}(t), j = 1, 2, \ldots, 6$, can be obtained by integrating the pressure on the wetted body surface:

$$f_j^{(2)}(t) = \iint_{S_B} p^{(2)} n_j \, dS + \iint_{S_\zeta(t)} (p^{(1)} - \rho_0 g z) n_j \, dS, \tag{3.2}$$

where $(n_1, n_2, n_3) = \boldsymbol{n}$, $(n_4, n_5, n_6) = \boldsymbol{r} \times \boldsymbol{n}$, and S_B and $S_\zeta(t)$ are respectively the mean and time-varying portions of the instantaneous wetted body surface.

For a harmonic incident wave, the second-order forces and moments contain double-frequency and steady components:

$$f_j^{(2)}(t) = \mathrm{Re}\{F_j^{(2)} e^{-2i\omega t}\} + \bar{F}_j^{(2)}. \tag{3.3}$$

The double-frequency forces and moments can be further split into those due to contributions from the quadratic products of the first-order potential, $F_1^{(2)}$, and those due to the second-order potential, $F_2^{(2)}$; i.e. $F_j^{(2)} = F_{j1}^{(2)} + F_{j2}^{(2)}$. These are given, for wall-sided bodies, by

$$F_{j1}^{(2)} = -\tfrac{1}{4}\rho_0 \left\{ \iint_{S_B} (\nabla \phi^{(1)})^2 n_j \, dS + \frac{\omega^2}{g} \int_{W_0} (\phi^{(1)})^2 n_j \, dl \right\}, \tag{3.4}$$

$$F_{j2}^{(2)} = 2i\omega\rho_0 \iint_{S_B} \phi^{(2)} n_j \, dS, \tag{3.5}$$

where W_0 is the mean waterline. The mean second-order component is

$$\bar{F}_j^{(2)} = -\tfrac{1}{4}\rho_0 \left\{ \iint_{S_B} |\nabla \phi^{(1)}|^2 n_j \, dS - \frac{\omega^2}{g} \int_{W_0} |\phi^{(1)}|^2 n_j \, dl \right\}. \tag{3.6}$$

For vertically axisymmetric bodies, the surface integrals can be reduced to line integrals along ∂B by integrating in θ and using orthogonality. Thus, for example, the horizontal force component, $F_{11}^{(2)}$, can be written as

$$\begin{aligned} F_{11}^{(2)} = & -\frac{\rho_0 a n_\rho \omega^2}{4g} \sum_{n=0}^{\infty} \frac{2\pi}{\epsilon_n} \phi_n^{(1)} \phi_{n+1}^{(1)} \Big|_{z=0} \\ & -\tfrac{1}{4}\rho_0 \sum_{n=0}^{\infty} \int_{\partial B} dl \, \rho n_\rho \left[\frac{2\pi}{\epsilon_n} \left(\frac{\partial \phi_n^{(1)}}{\partial \rho} \frac{\partial \phi_{n+1}^{(1)}}{\partial \rho} + \frac{\partial \phi_n^{(1)}}{\partial z} \frac{\partial \phi_{n+1}^{(1)}}{\partial z} \right) + \frac{\pi n(n+1)}{\rho^2} \phi_n^{(1)} \phi_{n+1}^{(1)} \right], \end{aligned} \tag{3.7}$$

If the body is not wall-sided, an extra factor, $(1 - n_z^2)^{-\frac{1}{2}}$, appears in the waterline terms.

For the free-surface elevation, $\zeta(t)$, we expand the exact free-surface condition in a Taylor expansion about $z = 0$, and obtain the second-order elevation

$$\zeta^{(2)}(t) = \left[\frac{-1}{2g} (\nabla \Phi^{(1)})^2 + \frac{1}{g^2} \frac{\partial \Phi^{(1)}}{\partial t} \frac{\partial^2 \Phi^{(1)}}{\partial t \partial z} - \frac{1}{g} \frac{\partial \Phi^{(2)}}{\partial t} \right]_{z=0}. \tag{3.8}$$

As with the velocity potential, $\zeta^{(2)}(t)$ can be decomposed into a time-independent term, $\bar{\eta}^{(2)}$, and a double-frequency term of amplitude $\eta^{(2)}$, which in turn can be written as a sum of contributions from the first-order ($\eta_1^{(2)}$) and second-order ($\eta_2^{(2)} = \eta_D^{(2)} + \eta_I^{(2)}$) potentals:

$$\zeta^{(2)}(t) = \mathrm{Re}\,[(\eta_1^{(2)} + \eta_2^{(2)})\,\mathrm{e}^{-2\mathrm{i}\omega t}] + \bar{\eta}^{(2)}, \tag{3.9}$$

and from (3.8):

$$\eta_1^{(2)} = \left[\frac{-1}{4g}(\nabla\phi^{(1)})^2 - \frac{\omega^2}{2g^2}\phi^{(1)}\frac{\partial\phi^{(1)}}{\partial z}\right]_{z=0}, \tag{3.10}$$

$$\eta_2^{(2)} = \eta_D^{(2)} + \eta_I^{(2)} = \frac{2\mathrm{i}\omega}{g}[\phi_D^{(2)} + \phi_I^{(2)}]_{z=0}, \tag{3.11}$$

$$\bar{\eta}^{(2)} = \left[\frac{-1}{4g}|\nabla\phi^{(1)}|^2 + \frac{\omega^2}{2g^2}\phi^{(1)}\frac{\partial\phi^{(1)*}}{\partial z}\right]_{z=0}. \tag{3.12}$$

If only integrated second-order quantities such as forces are required, an alternative method (Molin 1979; Lighthill 1979), which does not require the solution for $\phi_D^{(2)}$ explicitly, is to apply Green's theorem with the use of an assisting radiation potential, ψ_j, which satisfies the first-order boundary-value problem (2.4) at double-frequency, with the body boundary condition

$$\frac{\partial\psi_j}{\partial n} = n_j, \quad \text{on the body } (S_B); \quad j = 1, 2, \ldots, 6. \tag{3.13}$$

Applying Green's identity to $\phi_D^{(2)}$ and ψ_j, and taking advantage of the boundary conditions they satisfy, we obtain

$$\iint_{S_B} \phi_D^{(2)} n_j \,\mathrm{d}S = -\iint_{S_B} \psi_j \frac{\partial\phi_I^{(2)}}{\partial n}\,\mathrm{d}S + \frac{1}{g}\iint_{S_F} q\psi_j \,\mathrm{d}S, \tag{3.14}$$

so that the second-order forces are expressed in terms of first-order potentials only. For axisymmetric bodies, the free-surface integral in (3.14) has similar properties to that in (2.14) and the techniques of §2.4 are directly applicable. We remark that the computational effort involved in this indirect approach is not significantly different from the direct solution of §2, since in both cases an additional boundary-value problem at double-frequency ((2.14) or that for ψ) and an evaluation of similar free-surface integrals are involved.

For a uniform bottom-extended vertical cylinder, the first-order potentials can be expressed in closed form, so that semianalytic expressions (not involving solutions of integral equations) for the second-order forces and moments can be derived using (3.14). These are summarized in Appendix B, and provide useful comparisons for the numerical results of §2 for this geometry.

4. Numerical results and discussion

For illustration we consider the diffraction of plane monochromatic waves by two axisymmetric geometries: (*a*) a bottom-seated uniform vertical cylinder (radius a, depth $h = a$) for which semianalytic solutions for the forces are available (Appendix B); and (*b*) a conical island or gravity platform (waterplane radius a, depth $h = a$, toe angle 60°) where second-order effects are expected to be particularly important.

The integral equations (2.14) and (2.38) for the second- and first-order problems

$\nu a =$	1.2	2.0	2.8
exact	2.6282	1.6281	1.0529
$N_P = 10$	2.6250	1.6243	1.0481
20	2.6276	1.6271	1.0515
30	2.6281	1.6276	1.0520

TABLE 1. Magnitude of the first-order horizontal diffraction force, $|F_x^{(1)}|/\rho g a^2 A$, on a uniform vertical cylinder ($a/h = 1$) for different frequencies, $\nu a \equiv \omega^2 a/g$, as a function of the number of cosine-spaced segments, N_P, on the body, compared to exact values.

respectively are discretized and solved numerically following a standard procedure: (i) approximate the body contour, ∂B, by N_P straight line segments; (ii) assume constant values for the potential, $\phi_{Dn}^{(2)}$, or ring-source strength, σ_n, over each segment; (iii) collocate the equations at the centre of each segment to obtain a system of linear algebraic equations for the segment unknowns, which is then solved. In calculating the influence coefficients, the singularities of the kernels in §2.3 are subtracted out and integrated analytically. The sources of numerical error are those associated with: (i) the truncation to a finite number, N, of Fourier modes in θ; (ii) the assumed constant variations of the unknowns over each segment; and (iii) the geometric approximation of the body contour by N_P piecewise linear segments.

For the present geometries, the body contours are described exactly by straight segments, and the numerical errors are controlled by proper choices of N_P and N. Table 1 shows the errors in the modulus of the first-order horizontal diffraction force on the uniform cylinder as a function of N_P ($N_W = 20$ is used for the evaluation of the ring-source Green functions). To describe the more rapid variations near the free surface (especially for the second-order potential), cosine-spaced segments (with smaller lengths near the free surface) are used in all our calculations. The convergence with N_P is approximately quadratic. Hereafter, $N_P = 20$ segments are used for both the first- and second-order problems.

To show the convergence with increasing numbers, $n \leqslant N$, of azimuthal Fourier modes, we tabulate the modal amplitudes of the first- and second-order potentials on the vertical cylinder at $(\rho, z) = (a, 0)$ (which are proportional to the run-up) in table 2. For comparison, the amplitudes of the modes of the second-order incident and diffraction potentials are given separately. From partial wave decompositions of the incident waves, it is clear that the mode number beyond which the amplitudes attenuate rapidly increases with increasing frequency. This is seen for the larger $\omega^2 a/g \equiv \nu a$ as well as for the double-frequency potentials. It is of interest to note the large magnitudes and relatively slow decrease of $|\eta_{Dn}^{(2)}|$ compared to the double-frequency incident wave. In all our calculations up to $\nu a \approx O(3)$, $N = 9$ and 14 are used respectively for the linear and second-order problems.

A significant portion of the computational effort is in the evaluation of the free-surface integral in (2.14). For the free-surface forcing pressure terms, q_n (2.15), $\phi^{(1)}$ is calculated from first-order source strengths via (2.37) and its first and second derivatives from direct differentiation of (2.37). The Rankine part and its derivatives are evaluated analytically from (2.18). With the use of constant-strength segments, the potential and its derivatives on the free surface from (2.37) are not accurate in a small neighbourhood (of the order of a segment length) near the intersection with the body (e.g. Korsmeyer 1988). In practice, we obtain $\phi_z^{(1)}(a, 0)$ and $\phi_\rho^{(1)}(a, 0)$ from $\phi^{(1)}(a, 0)$ using free-surface and body boundary conditions respectively; $\phi_{\rho\rho}^{(1)}(a, 0)$

$\nu a =$	1.2			2.0			2.8		
	$\lvert\eta_n^{(1)}\rvert$	$\lvert\eta_{Dn}^{(2)}\rvert$	$\lvert\eta_{In}^{(2)}\rvert$	$\lvert\eta_n^{(1)}\rvert$	$\lvert\eta_{Dn}^{(2)}\rvert$	$\lvert\eta_{In}^{(2)}\rvert$	$\lvert\eta_n^{(1)}\rvert$	$\lvert\eta_{Dn}^{(2)}\rvert$	$\lvert\eta_{In}^{(2)}\rvert$
$n=0$	0.6339	0.3242	0.0966	0.5308	1.1600	0.0793	0.4704	0.4404	0.0024
1	1.3028	0.8133	0.5301	1.1048	1.1375	0.0471	0.9477	2.3280	0.0400
2	0.8704	0.7719	0.5810	1.1422	1.1666	0.1358	1.0170	1.9287	0.0191
3	0.2018	0.3300	0.3201	0.6365	0.9640	0.1786	1.0089	1.6163	0.0265
4	0.0339	1.4545	0.1215	0.1639	0.2415	0.1236	0.5051	1.2758	0.0473
5	0.0047	1.4183	0.0355	0.0338	0.8139	0.0608	0.1431	0.6720	0.0405
6	0.0005	0.5586	0.0085	0.0059	1.2414	0.0235	0.0341	0.3541	0.0246
7	0.0001	0.1152	0.0017	0.0009	1.0073	0.0076	0.0070	1.0061	0.0118
8	0.5×10^{-5}	0.0194	0.0003	0.0001	0.5904	0.0021	0.0013	1.0968	0.0048
9	0.3×10^{-6}	0.0029	0.5×10^{-4}	0.1×10^{-4}	0.2228	0.0005	0.0002	0.7860	0.0016
10	0.2×10^{-7}	0.0004	0.6×10^{-5}	0.1×10^{-5}	0.0490	0.0001	0.3×10^{-4}	0.4555	0.0005
11	0.1×10^{-8}	0.0001	0.8×10^{-6}	0.1×10^{-6}	0.0086	0.2×10^{-4}	0.4×10^{-5}	0.2263	0.0001
12	*	0.6×10^{-5}	0.9×10^{-7}	0.1×10^{-7}	0.0014	0.4×10^{-5}	0.5×10^{-6}	0.0862	0.3×10^{-4}
13	*	0.6×10^{-6}	0.1×10^{-7}	0.9×10^{-9}	0.0002	0.6×10^{-6}	0.5×10^{-7}	0.0208	0.8×10^{-5}
14	*	0.5×10^{-7}	0.1×10^{-8}	*	0.2×10^{-4}	0.9×10^{-7}	0.5×10^{-8}	0.0036	0.2×10^{-5}

TABLE 2. Convergence of the linear and second-order surface elevation angular modal amplitudes (normalized by A and A^2/a respectively) on the circumference ($\rho = a$) of a uniform vertical cylinder ($a/h = 1$) for $\nu a = 1.2$, 2.0 and 2.8. (* indicates values less than 10^{-10}).

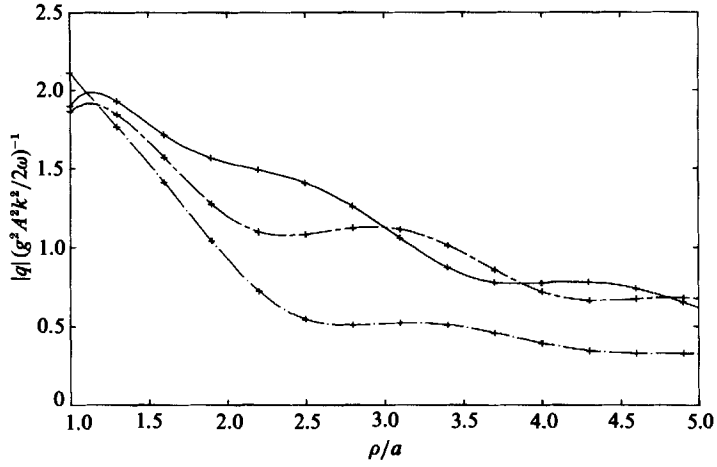

FIGURE 1. Comparison between analytic and computed results (+) for the amplitude of the first three modes of the second-order free-surface forcing pressure outside a uniform vertical cylinder ($h = a$, $\nu a = 2$) as a function of radial distance. The curves are analytic results for: q_0 (—·—); q_1 (——); and q_2 (– – –).

from three-point differencing of $\phi_\rho^{(1)}$ on the free surface and the body; and $\phi_{zz}^{(1)}$ $(a, 0)$ from applying Laplace's equation at the intersection point. The values for $0 < (r-a)/a \ll 1$ are then obtained by three-point quadratic interpolations between values on the body and those on the free surface a small distance away. For cosine-spaced body segments, the typical relative errors in q_n we compute are $O(0.1\%)$. Figure 1 shows the comparisons between computed results and analytic solutions (cf. Appendix B) for the first three modes of the forcing pressure outside a uniform cylinder for $\nu a = 2$. The slowly decaying and oscillatory behaviour of the profiles are quite evident.

$\nu a =$	1.2		2.0		2.8	
	$\lvert F_2^{(2)}\rvert$	$\lvert M_2^{(2)}\rvert$	$\lvert F_2^{(2)}\rvert$	$\lvert M_2^{(2)}\rvert$	$\lvert F_2^{(2)}\rvert$	$\lvert M_2^{(2)}\rvert$
exact	2.263	1.239	2.694	1.439	4.229	2.429
$(b-a)/h = 2$	2.258	1.237	2.663	1.430	4.193	2.418
3	2.262	1.238	2.691	1.437	4.227	2.429
4	2.263	1.238	2.694	1.439	4.231	2.431

TABLE 3. Magnitude of the second-order potential horizontal force and overturning moment (normalized by $\rho g a A^2$ and $\rho g a^2 A^2$ respectively) on a uniform vertical cylinder, $a/h = 1$. The results are for different partition radii b for the free-surface integral evaluation compared to semianalytic solutions (Appendix B).

The free-surface integral in (2.14) is calculated using the method of §2.4. To estimate the convergence of the integral with the partition radius b, we consider a typical local mode in the second term of (2.30). Using the addition theorem for K_0:

$$K_0(\kappa_m R) = \sum_{n=0}^{\infty} \epsilon_n I_n(\kappa_m \rho') K_n(\kappa_m \rho) \operatorname{cosn}(\theta - \theta'), \tag{4.1}$$

it is clear that for ρ' on the body, the decay of the local modes with ρ is exponential with a rate given by $\kappa_m \rho$ or in fact ρ/h according to (2.32). In general, for a given tolerance, we select a fixed $(b-a)/h$ to control the error associated with neglected evanescent waves in the outer integral. Table 3 shows typical convergence of results with $(b-a)/h$ for the second-order potential horizontal force and overturning moment (with respect to the bottom) on a uniform vertical cylinder ($a/h = 1$). It is seen that a partition radius of $b-a \sim 3h$ is adequate for three significant decimals of accuracy and is used in later computations. The accuracy with relatively small numerical integration requirements again underscores the efficacy of the method of §2.4 compared to methods that have only algebraic convergence.

We now turn to the results for the two geometries. Table 4 shows the first- and second-order forces and moments on the uniform circular cylinder (computed from pressure integration on the body) compared to semianalytic results (Appendix B). For the evaluation of the second-order mean ($\bar{F}_x^{(2)}$ and $\bar{M}_y^{(2)}$) and that part of the double-frequency ($F_{x1}^{(2)}$ and $M_{y1}^{(2)}$) forces and moments given by the first-order potential, the gradients of the linear potential on the body are required and are calculated by three-point centred differences of collocation point values. The errors in table 4 increase somewhat with frequency but are less than 1% for all the quantities shown. In all cases for the force, the contribution of the second-order potential is larger than that of quadratic products of first-order quantities. However, these two effects are generally out of phase so that the net second-order excitations are relatively small compared with the linear quantities but increase with increasing wave frequency. Thus for moderately steep waves, say $kA \sim 0.2$, the double-frequency second-order force amplitude is only about 4–16% for $\nu a = 1.2$–2.8. The situation for the overturning moment is similar but with somewhat smaller ratios of $M_{y2}^{(2)}$ to $M_{y1}^{(2)}$. This is related to the relative centres of pressure of the different pressure components (see figures 3 and 4).

The magnitudes of the first- and second-order force coefficients are plotted in figure 2 as a function of incident frequency. The comparisons with semianalytic results are uniformly good except for small discrepancies in a neighbourhood of $\nu a \approx 2.4$ which

$\nu a =$	1.2		2.0		2.8	
$F_x^{(1)}$	0.708,	−2.531	−0.264,	−1.606	−0.746,	−0.743
	0.708,	−2.531	−0.264,	−1.606	−0.745,	−0.742
$\bar{F}_x^{(2)}$	0.826		0.711		0.656	
	0.826		0.711		0.655	
$F_{x1}^{(2)}$	−1.648,	−0.308	−1.094,	0.849	0.892,	1.341
	−1.648,	−0.305	−1.076,	0.846	0.887,	1.345
$F_{x2}^{(2)}$	2.259,	−0.136	1.972,	−1.835	−2.209,	−3.606
	2.258,	−0.135	1.973,	−1.830	−2.208,	−3.604
$F_x^{(2)}$	0.611,	−0.444	0.878,	−0.986	−1.317,	−2.265
$M_y^{(1)}$	0.401,	−1.431	−0.165,	−1.004	−0.511,	−0.509
	0.400,	−1.431	−0.165,	−1.003	−0.510,	−0.509
$\bar{M}_y^{(2)}$	0.870		0.822		0.777	
	0.870		0.823		0.778	
$M_{y1}^{(2)}$	−1.485,	−0.385	−1.063,	0.801	0.835,	1.268
	−1.485,	−0.382	−1.044,	0.797	0.829,	1.272
$M_{y2}^{(2)}$	1.201,	−0.303	1.041,	−0.993	−1.360,	−2.012
B	1.200,	−0.302	1.042,	−0.990	−1.360,	−2.013
$M_y^{(2)}$	−0.284,	−0.688	−0.022,	−0.192	−0.525,	−0.744

TABLE 4. Real and imaginary parts (real, imag) of the first- and second-order horizontal force and overturning moment (with respect to the bottom) of a uniform vertical cylinder ($a/h = 1$) obtained by direct pressure integration on the body. For comparison, semianalytic solutions obtained using assisting potentials (Appendix B) are given on the first rows. (The quantities $F^{(1)}$, $M^{(1)}$, $F^{(2)}$ and $M^{(2)}$ are normalized by $\rho g a^2 A$, $\rho g a^3 A$, $\rho g a A^2$ and $\rho g a^2 A^2$ respectively.)

corresponds to the first irregular frequency of the integral equation (2.38). (The frequency is given by the homogeneous interior Dirichlet solution at the first zero of $J_0(ka)$ at $ka \approx 2.405$ or $\nu a \approx 2.366$. The effects of the irregular frequencies, ν, associated with (2.14) which are one-fourth those of (2.38) are much weaker.) The force components due to the second-order potential are major portions of the total second-order quantities and their magnitudes relative to the other second-order contributions increase with increasing frequency. Thus, in no situation is it valid to ignore $F_2^{(2)}$ in favour of quadratic contributions of the first-order potential. This invalidates many recent engineering estimates of second-order wave effects on structures (e.g. Herfjord & Nielsen 1986; Petrauskas & Liu 1987) wherein the second-order potentals were ignored. Note that both $F_2^{(2)}$ and $M_2^{(2)}$ blow up as $\nu a = \nu h \to 0$, and the second-order result becomes invalid. This is related to failure of Stokes' expansion (see (2.3)) as $kh \ll 1$ for fixed kA. As pointed out earlier, $F_2^{(2)}$ and $F_1^{(2)}$ (as well as the moments) are generally out of phase, so that the net double-frequency excitation amplitude is usually smaller than that of $F_2^{(2)}$ and important only for steep incident waves.

Unlike earlier work such as Molin (1979) and Eatock Taylor & Hung (1987), we obtain the second-order potential explicitly so that useful local second-order quantities such as pressure distribution, velocities and wave run-up are also available. Figures 3(*a*) and 3(*b*) show the amplitudes of the linear and components of the second-order pressure distributions on the cylinder on the lee ($\theta = 0$) and

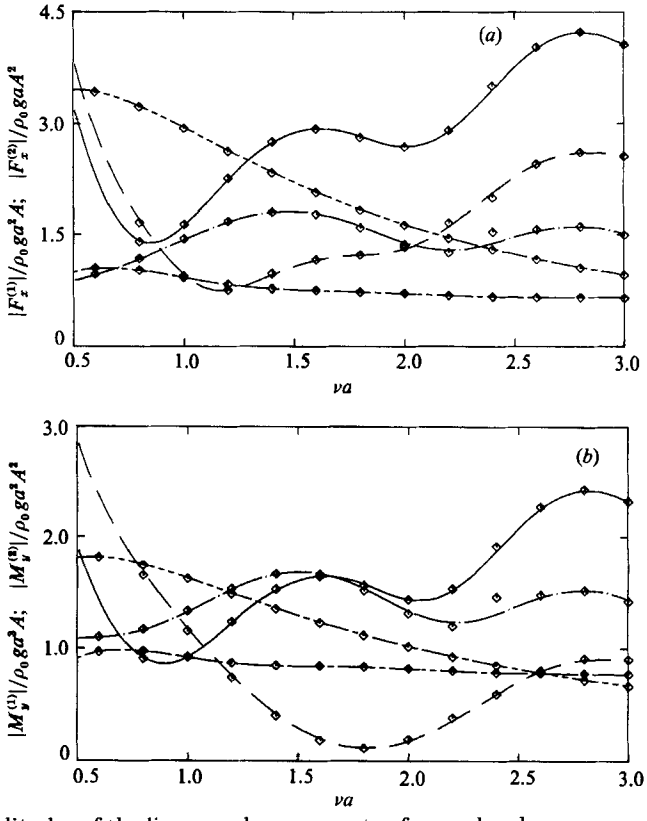

FIGURE 2. Amplitudes of the linear and components of second-order wave excitations on a uniform vertical cylinder ($a = h$) as a function of incident frequency, νa. The curves are for semianalytic solutions for: $|F^{(1)}|$ (———); $\bar{F}^{(2)}$ (— — —); $|F_1^{(2)}|$ (—·—); $|F_2^{(2)}|$ (———); and $|F_1^{(2)}+F_2^{(2)}|$ (———). Results from pressure integration are denoted by symbols (◇). (*a*) Horizontal force, F_x; and (*b*) pitch moment with respect to the bottom, M_y.

weather ($\theta = \pi$) sides respectively for $\nu a = 2$. Analytic results, where available (from (B 1)), are also shown. The pressures $p_1^{(2)}$ and $\bar{p}^{(2)}$ which are due to quadratic products of the first-order potential, as well as the pressure due to $\phi_1^{(2)}$ attenuate with depth with a rate of $\sim 2k$, whereas the pressure associated with the second-order double-frequency free waves (ϕ_H) has a decay rate given by $k_2 \sim 4k$. On the other hand, the portion of the nonlinear potential second-order pressure, $p_2^{(2)}$ which is forced by the inhomogenous surface term (2.6), has a much slower attenuation with depth dictated by (2.6). This is especially evident on the weather side. The phenomenon can be seen in general from the far-field behaviour of ϕ_P, (2.10), where the depth-dependence of the potential varies from being a constant on the weather side ($\theta = \pi$) to cosh $2k(z+h)$ on the lee side.

For longer waves, the situation is even more interesting, where the pressure may not decrease (monotonically) with depth and the minimum $p_2^{(2)}$ may not in general be at the bottom. This is shown in figure 4 for the case of $\nu a = 1.2$, for different circumferential positions along the cylinder. Along the leeward ($\theta = 0$) edge, the second-order potential pressure first decreases with depth, reaching a minimum at around middraught and then begins to increase towards the bottom. At the waveward quarter ($\theta = 3\pi/4$) the pressure has a minimum close to the surface and then *increases* monotonically with depth.

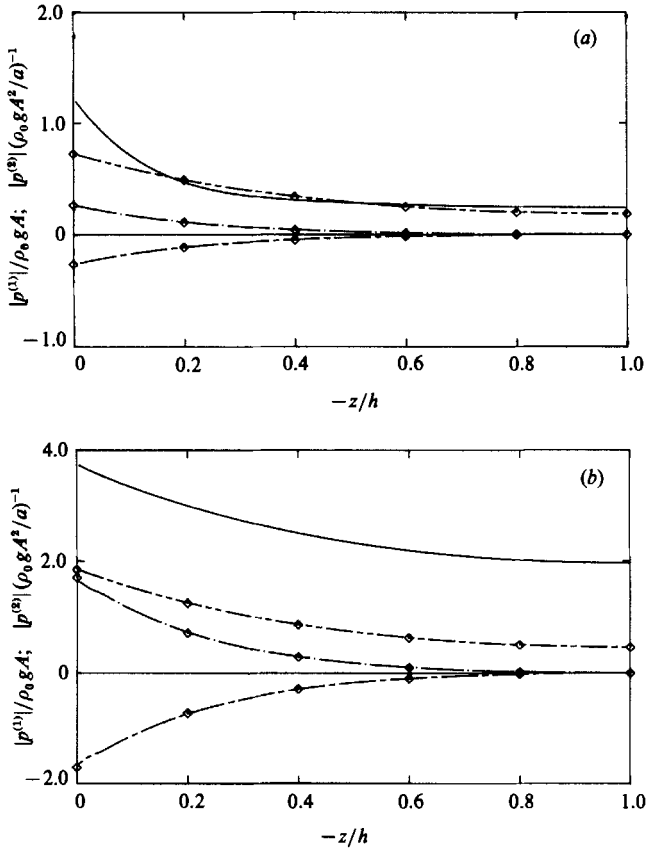

FIGURE 3. Modulus of the linear and components of second-order hydrodynamic pressure on the side of a uniform vertical cylinder ($h = a$, $\nu a = 2$) on (*a*) the lee side ($\theta = 0$); and (*b*) the weather side ($\theta = \pi$). The curves are computed results for: $|p^{(1)}|$ (———); $\bar{p}^{(2)}$ (— — —); $|p_1^{(2)}|$ (—·—); and $|p_2^{(2)}|$ (———). Analytic results obtained from the linear potential are denoted by symbols (◇).

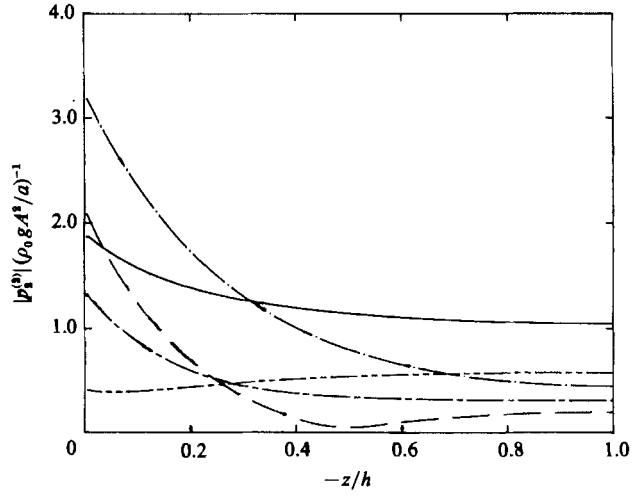

FIGURE 4. Modulus of the (double-frequency) hydrodynamic pressure due to the second-order potential on the side of a uniform vertical cylinder ($h = a$, $\nu a = 1.2$) at different angular positions: $\theta = 0$ (———); $\theta = \frac{1}{4}\pi$ (—·—); $\theta = \frac{1}{2}\pi$ (— — —); $\theta = \frac{3}{4}\pi$ (— — —); and $\theta = \pi$ (———).

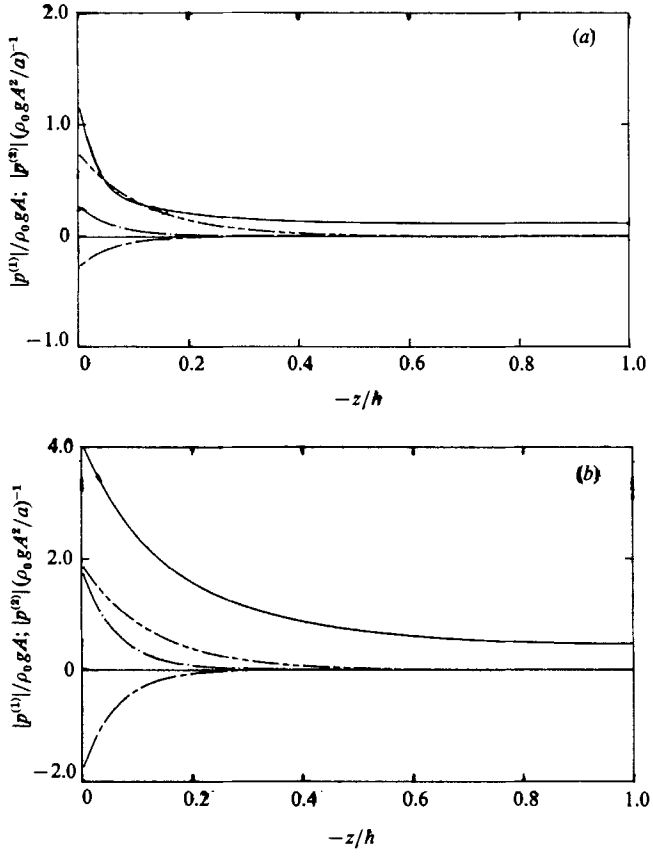

FIGURE 5. Modulus of the linear and components of second-order hydrodynamic pressure on the side of a uniform vertical cylinder ($h = 4a$, $\nu a = 2$) on (a) the lee side ($\theta = 0$); and (b) the weather side ($\theta = \pi$). The curves are computed results for: $|p^{(1)}|$ (———); $\bar{p}^{(2)}$ (———); $|p_1^{(2)}|$ (—·—); and $|p_2^{(2)}|$ (———).

For deeper water, the total hydrodynamic pressure may be dominated by that due to the second-order potential. Figure 5 shows the pressure distributions on a uniform cylinder of depth $h = 4a$ at $\nu a = 2$. As expected, all pressure components given by $\phi^{(1)}$ ($\phi_1^{(2)}$ or ϕ_H) attenuate exponentially while $p_2^{(2)}$ (which is proportional to ϕ_P at deeper depths) has only an algebraic-like decay with depth. This has a very important consequence for the forces on deep-draught bodies. Figure 6 shows the horizontal force components on a uniform cylinder of varying depth h/a for $\nu a = 2$. With the attenuation of linear-potential pressures with depth, the quantities $F_x^{(1)}$ and $F_{x1}^{(2)}$ (as well as forces due to $\phi_1^{(2)}$ and ϕ_H) reach constant values rapidly as h/a increases. The force due to the second-order potential, ϕ_P, however, continues to increase in magnitude and converges to a constant asymptotic very slowly. For information, the magnitudes of the first-and second-order components of the free-surface elevation on the cylinder (at $\theta = \pi$) are also plotted, which show that the increase in $F_{x2}^{(2)}$ is not due to the magnitude of the potential on the surface. For truncated cylindrical bodies, this phenomenon gives rise to unexpected second-order *vertical* forces even when $\nu H > O(1)$, where H is the draught of the body (Kim & Yue 1988).

We next show the first- and second-order run-up on the uniform cylinder as a

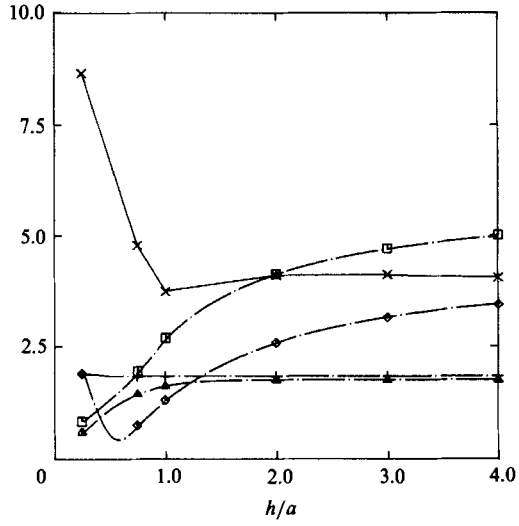

FIGURE 6. Amplitudes of the linear and components of second-order horizontal force and run-up (at $\theta = \pi$) for uniform vertical cylinders ($\nu a = 2$) as a function of the depth, h. Connected symbols are for computed values of: $|F^{(1)}|/\rho_0 g a^2 A$ (△); $|F_2^{(2)}|/\rho_0 g a A^2$ (□); $|F_1^{(2)} + F_2^{(2)}|/\rho_0 g a A^2$ (◇); $|\eta^{(1)}|/A$ (+); and $|\eta_2^{(2)}|a/A^2$ (×). Analytic solutions are represented by the curves (—·—).

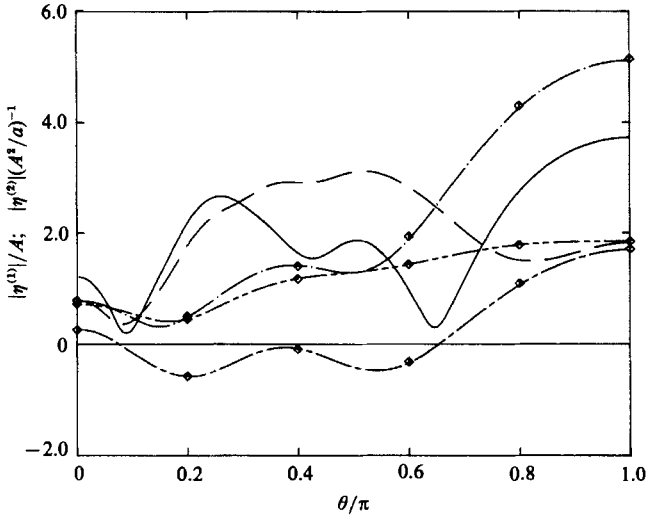

FIGURE 7. Amplitudes of the linear and components of second-order free-surface elevations (run-up) on a uniform vertical cylinder ($h = a$, $\nu a = 2$) as a function of the azimuthal angle, θ. The curves are for computed values for: $|\eta^{(1)}|$ (— — —); $\bar{\eta}^{(2)}$ (— — —); $|\eta_1^{(2)}|$ (—·—); $|\eta_2^{(2)}|$ (———); and $|\eta_1^{(2)} + \eta_2^{(2)}|$ (———). Analytic results obtained from the linear potential are denoted by symbols (◇).

function of the azimuthal angle θ for $\nu a = 2$ (figure 7). The amplitudes of the run-up components generally increase from the lee ($\theta = 0°$) to weather side, whereas $\eta_2^{(2)}$ has another maximum at the lee quarter. The relative magnitudes and phases between $\eta_1^{(2)}$ and $\eta_2^{(2)}$ depend on θ, and in general the total double-frequency run-up can be several times larger than the second-order mean set-up (down), which itself has a trend similar to $\eta_1^{(2)}$, with a maximum set-up on the weather side and set-down along

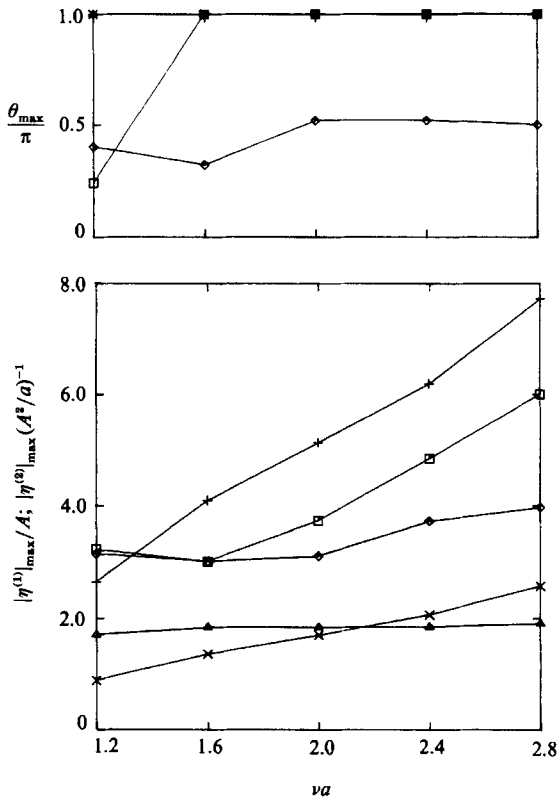

FIGURE 8. Maximum amplitudes (over θ) and the positions of the maxima (θ_{max}) of the linear and components of second-order wave run-up on a uniform vertical cylinder ($h = a$) as a function of incident frequency, νa. The symbols are for: $|\eta^{(1)}|$ ($\triangle$); $\bar{\eta}^{(2)}$ ($\times$); $|\eta_1^{(2)}|$ ($+$); $|\eta_2^{(2)}|$ ($\square$); and $|\eta_1^{(2)}+\eta_2^{(2)}|$ ($\diamond$).

the leeward portion of the cylinder. The general behaviour of the various run-up components is sensitive to the incident wave frequency. In figure 8, we plot the maximum amplitude, over θ, and the position of the maximum (θ_{max}) of these components as a function of νa. Except for the lower frequency, the maximum $|\eta_1^{(2)}|$ is greater than $|\eta_2^{(2)}|$ by almost a constant factor, while both quantities as well as the maximum $|\bar{\eta}^{(2)}|$ (which are all for $\bar{\eta}^{(2)} > 0$) tend to increase with frequency. The maximum net double-frequency amplitude $|\eta_1^{(2)} + \eta_2^{(2)}|$ is less sensitive to frequency, as is the case for the linear run-up, $|\eta^{(1)}|$. The dependence on water depth has been plotted in figure 6 for $\nu a = 2$. In general, the amplitudes, including $|\eta_2^{(2)}|$, are not sensitive to increasing depth beyond $\nu h > \sim 2$. On the other hand $\eta_2^{(2)}$increases rapidly in shallow water as a consequence of Stokes' expansion for long waves, as pointed out earlier.

We next turn to results for a bottom-seated truncated vertical cone (waterplane radius a, water depth $h = a$, and a toe angle of 60°). Such a geometry has been proposed for gravity platforms in the Arctic (e.g. Sarpkaya & Isaacson 1981), or may be considered as model for a circular island. In this case, the non-vertical body wall is expected to lead to more important second-order effects.

Figure 9 shows the magnitude of the components of horizontal and vertical forces and overturning moment (with respect to the bottom centre) on such a body. As a

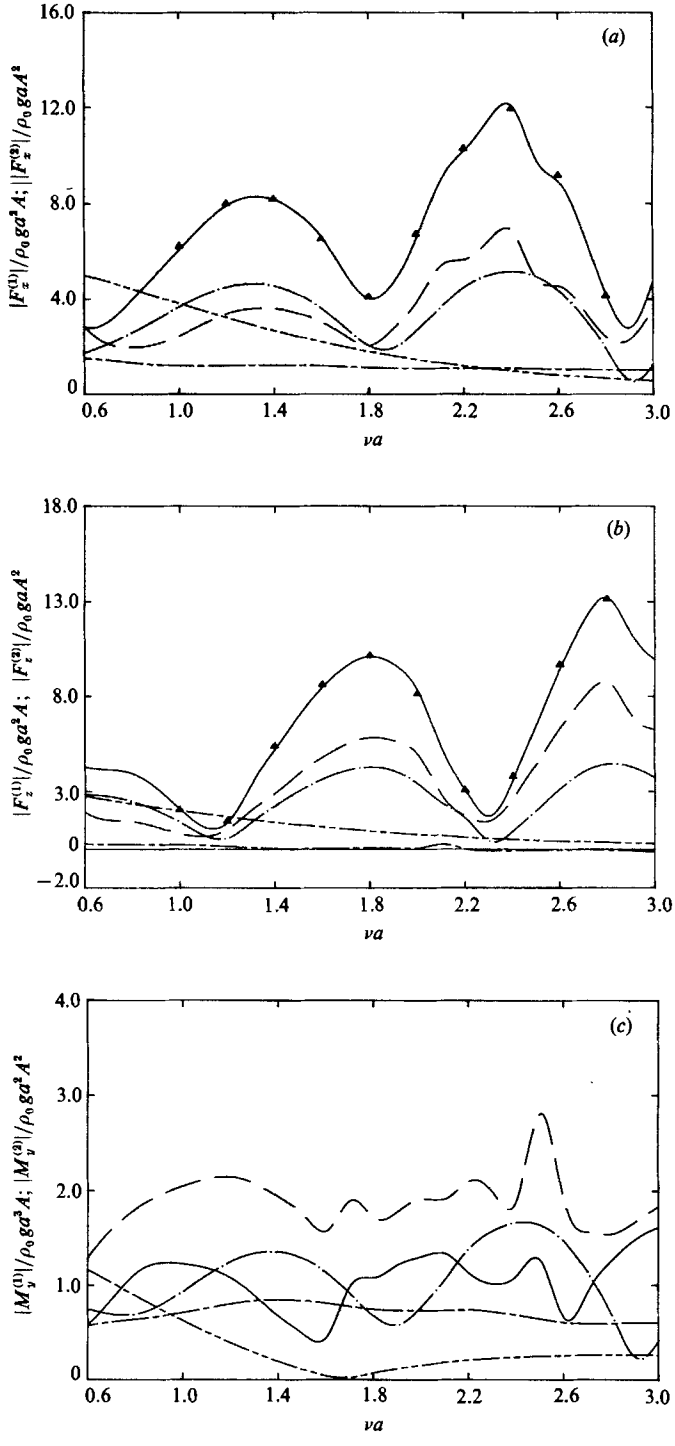

FIGURE 9. Amplitudes of the linear and components of second-order wave excitations on a truncated vertical cone ($h = a$, toe angle 60°) as a function of incident frequency, νa. The curves are for results computed from pressure integration for: $|F^{(1)}|$ (———); $\bar{F}^{(2)}$ (– – –); $|F_1^{(2)}|$ (—·—); $|F_2^{(2)}|$ (———); and $|F_1^{(2)}+F_2^{(2)}|$ (———). The symbols (△) denote results calculated from (3.14). (*a*) Horizontal force, F_x; (*b*) vertical force, F_z; and (*c*) pitch moment with respect to the bottom, M_y.

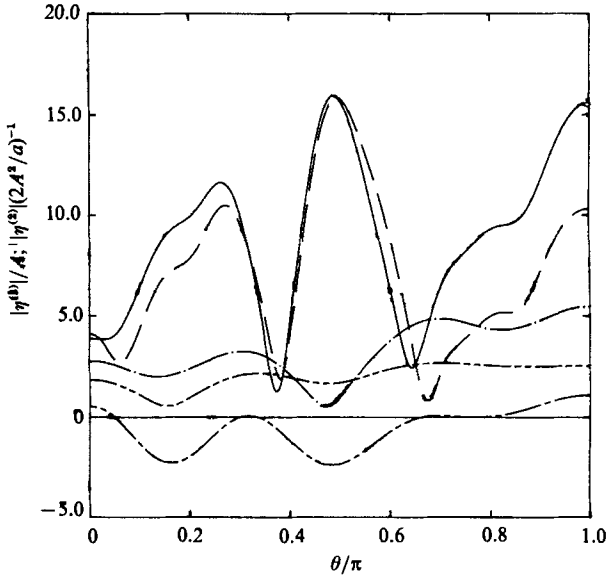

FIGURE 10. Amplitudes of the linear and components of second-order free-surface elevations (run-up) on a truncated vertical cone ($h = a$, toe angle 60°, $\nu a = 2$) as a function of the azimuthal angle, θ. The curves are for computed values for: $|\eta^{(1)}|$ (———); $\bar{\eta}^{(2)}$ (———); $|\eta_1^{(2)}|$ (—·—); $|\eta_2^{(2)}|$ (———); and $|\eta_1^{(2)} + \eta_2^{(2)}|$ (———). Note that a different scale is used for plotting second-order amplitudes.

check, the results for $|F_{x2}^{(2)}|$ and $|F_{z2}^{(2)}|$ obtained independently using assisting potentials, (3.14), are also plotted. These second-order potential forces dominate all other second-order contributions throughout the frequency range. Although the relative phases between $F_1^{(2)}$ and $F_2^{(2)}$ still cause the amplitudes to partially cancel, the net second-order double-frequency forces on the cone may be an appreciable part of the total excitation, especially for higher frequencies. For example, for wave slope of $kA = 0.2$, $|F_{x1}^{(2)} + F_{x2}^{(2)}|$ at $\nu a \approx 2.4$ and $|F_{z1}^{(2)} + F_{z2}^{(2)}|$ at $\nu a \approx 2.8$ are respectively 60% and 180% of the corresponding linear amplitudes at those frequencies. For the overturning moment, $M_2^{(2)}$ is comparable in magnitude with $M_1^{(2)}$ and they both oscillate with frequency. In this case, however, the components are roughly in phase and the net double-frequency moment is comparable with the linear moment only for steep waves (say $kA > \sim 0.25$ at $\nu a \sim 2.5$).

The run-up along the circumference of the cone is plotted in figure 10 for the first- and second-order double-frequency and steady components for $\nu a = 2$. The double-frequency run-up is much greater than that for the vertical cylinder and shows large variations along the waterline. The net amplitude is given essentially by the second-order potential component and has a maximum at the sides of the cone where it may be comparable with the first-order run-up there for $kA > \sim 0.13$. Again the detailed features depend very much on the specific incident frequency, and the results are summarized in figure 11 where the maxima, over θ, of the amplitudes of the various run-up components are plotted as a function of νa together with the positions ($\theta_{\max}$) of the respective maxima. Comparing to figure 8 for the vertical cylinder, we observe that: the magnitudes of the second-order components are *much* larger; $|\eta_1^{(2)}|_{\max}$ is now quite small compared with $|\eta_2^{(2)}|_{\max}$; the maximum total double-frequency run-up increases more rapidly with frequency; the locations of the maxima are more sensitive to frequency; and the interesting fact that the maxima of $|\bar{\eta}^{(2)}|$ are now all for mean set-down (i.e. $\bar{\eta}^{(2)} < 0$).

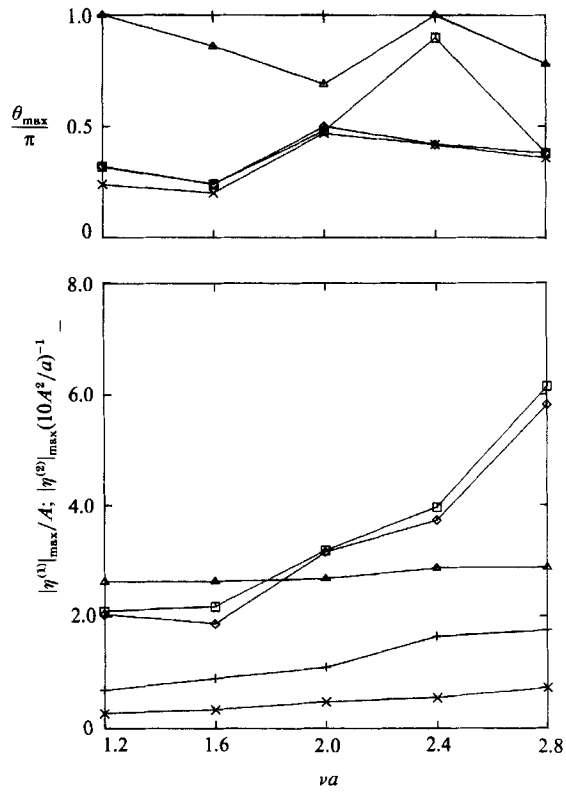

FIGURE 11. Maximum amplitudes (over θ) and the positions of the maxima (θ_{max}) of the linear and components of second-order wave run-up on a truncated vertical cone ($h = a$, toe angle 60°) as a function of incident frequency, νa. The symbols are for: $|\eta^{(1)}|$ (△); $\bar{\eta}^{(2)}$ (×); $|\eta_1^{(2)}|$ (+); $|\eta_2^{(2)}|$ (□); and $|\eta_1^{(2)} + \eta_2^{(2)}|$ (◇). Note that a different scale is used for plotting second-order amplitudes.

We have also calculated the components of the pressure on the cone. With the exception of a sharper rise of $p_2^{(2)}$ towards the free surface, the qualitative features are similar to those for the vertical cylinder and are not shown.

5. Conclusion

Using a general order ring-source boundary-integral equation method, the second-order diffraction problem for an axisymmetric body in the presence of plane monochromatic incident waves is solved for the nonlinear sum-frequency potential. An important part of the solution is the efficient and accurate calculation of the forcing term which requires the evaluation of an oscillatory and slowly decaying integral on the free surface. An approach that treats the entire local-wave-free outer region analytically is developed and shown to be efficacious. Although the second-order potential is solved explicitly, the present method is comparable in computational effort with existing approaches (Molin 1979; Lighthill 1979) which utilize fictitious assisting potentials to obtain global second-order quantities. An important benefit is that complete second-order local quantities such as pressure distributions and surface elevations are now available.

For illustration, the second-order diffraction problem for a uniform vertical cylinder and a truncated vertical cone are studied in some detail. In addition to

convergence tests with respect to truncation and discretizations, comparisons of the second-order forces and moments for both geometries with independent results obtained using assisting potentials confirm the validity and accuracy of the present calculations.

From our numerical examples, several important second-order diffraction features are observed:

(i) The *relative* importance of second-order effects generally increases with frequency, $\omega^2 a/g$, and with the draught of the body, $\omega^2 H/g$.

(ii) The second-order potential cannot be neglected in favour of quadratic contributions of the linear potential. Double-frequency results obtained without accounting for this potential will probably be inadequate in all but very specialized cases.

(iii) The second-order double-frequency diffraction potential can penetrate much deeper than even the linear (incident-frequency) potentials. The pressure or velocities associated with this nonlinear potential may not in general be negligible even for $|\omega^2 z/g| > O(1)$. In particular, the *vertical* force otherwise absent on a deep truncated cylinder can be non-trivial owing to this potential.

(iv) When the body sidewalls are outward sloping towards the bottom, such as in the case of a vertical cone, second-order effects such as run-up are amplified and may indeed be greater than first-order quantities for moderately steep incident waves.

The present method can be generalized to the case where the incident waves contain multiple frequency components (resulting in second-order potentials at the sums and differences of the component frequencies) as well as the radiation problem – these are considered in Part 2. For general three-dimensional bodies, (2.11) requires the two-dimensional free-surface integral:

$$I(x') = \iint_{S_F} q(\boldsymbol{x})\, G^+(\boldsymbol{x};\boldsymbol{x}')\, \mathrm{d}\boldsymbol{x}, \tag{5.1}$$

where q is given by (2.6) and $\phi_D^{(1)}$ in (2.6) can be given, say, by a source distribution on the body:

$$\phi_D^{(1)}(\boldsymbol{x}) = \iint_{S_B} \sigma(\boldsymbol{x}')\, G(\boldsymbol{x};\boldsymbol{x}')\, \mathrm{d}\boldsymbol{x}'. \tag{5.2}$$

Using the far-field asymptotic of G, (2.33), and the addition theorem for Hankel functions, we have after a simple expansion:

$$\begin{Bmatrix} G \\ \phi_D^{(1)} \end{Bmatrix} \sim \sum_{n=0}^{\infty} H_n(k\rho) \begin{Bmatrix} g_{Cn}(\boldsymbol{x}')\cos n\theta + g_{Sn}(\boldsymbol{x}')\sin n\theta \\ L_{Cn}\ \cos n\theta + \ L_{Sn}\ \sin n\theta \end{Bmatrix}, \quad k\rho \gg 1, \tag{5.3}$$

where g_{Cn}, g_{Sn} are known functions of the point $\boldsymbol{x}'$ on the body, and L_{Cn}, L_{Sn} are the Kochin functions:

$$\begin{Bmatrix} L_{Cn} \\ L_{Sn} \end{Bmatrix} = \iint_{S_B} \sigma(\boldsymbol{x}') \begin{Bmatrix} g_{Cn}(\boldsymbol{x}') \\ g_{Sn}(\boldsymbol{x}') \end{Bmatrix} \mathrm{d}\boldsymbol{x}'. \tag{5.4}$$

Using (5.2)–(5.4) in (5.1) in the local-wave-free far field, the θ-integral can be integrated explicitly, and (5.1) reduces to sums of one-dimensional integrals over the radial coordinate ρ of the forms (2.42), and the method of Appendix A is directly applicable.

This research is financially supported by the National Science Foundation and the Office of Naval Research. Portions of the computations were performed on the NSF sponsored Pittsburgh Supercomputer Center Cray X/MP. D.K.P.Y. also acknowledges partial support of the Henry L. Doherty Chair Professorship.

Appendix A. Evaluation of the triple-Henkel integrals (2.42)

We consider, as an example, the integral

$$I^1_{lmn}(x_0) = \int_{x_0}^{\infty} xH_l(x)\,H_m(x)\,H_n(\alpha x)\,\mathrm{d}x, \tag{A 1}$$

where $x_0 \equiv kb$, and $\alpha \equiv k_2/k$. To evaluate (A 1), we expand each Hankel function in polynomials of x_0/x, whose coefficients can be determined from an equivalent Chebyshev polynomial expansion for a specified equal-ripple error (Luke 1975):

$$H_n(x) = \left(\frac{2}{\pi x}\right)^{\frac{1}{2}} \mathrm{e}^{\mathrm{i}(x-\gamma_n)} \sum_i C_{ni}(x_0/x)^i, \quad i = 1, 2, \ldots, \tag{A 2}$$

where $\gamma_n \equiv (\frac{1}{2}n + \frac{1}{4})\pi$. The integral (A 1) can then be written as a triple sum:

$$I^1_{lmn} = A_{lmn} \sum_i \sum_j \sum_k C_{li}\,C_{mj}\,C_{nk}\,\alpha^{-k}\,x_0^{i+j+k} \int_{x_0}^{\infty} \frac{\mathrm{e}^{\mathrm{i}(2+\alpha)x}}{x^{i+j+k+\frac{1}{2}}}\mathrm{d}x, \tag{A 3}$$

where

$$A_{lmn} \equiv \frac{2\sqrt{2}}{\pi(\pi\alpha)^{\frac{1}{2}}} \mathrm{e}^{-\mathrm{i}(\gamma_l+\gamma_m+\gamma_n)}.$$

Using a change of variable, $y = (2+\alpha)x$, we obtain

$$I^1_{lmn} = B_{lmn} \sum_i \sum_j \sum_k \alpha^{-k}\,y_0^{i+j+k}\,C_{li}\,C_{mj}\,C_{nk}\,U(i+j+k), \tag{A 4}$$

where $y_0 \equiv (2+\alpha)x_0$, $B_{lmn} \equiv (2+\alpha)^{-\frac{1}{2}} A_{lmn}$, and U is defined to be the definite integral

$$U(n) \equiv \int_{y_0}^{\infty} \frac{\mathrm{e}^{\mathrm{i}y}}{y^{n+\frac{1}{2}}}\mathrm{d}y. \tag{A 5}$$

Upon integration by parts in (A 5), the following recurrence formula for $U(n)$ can be derived:

$$U(n) = \frac{\mathrm{e}^{\mathrm{i}y_0}}{(n-\frac{1}{2})\,y_0^{n-\frac{1}{2}}} + \frac{\mathrm{i}}{n-\frac{1}{2}} U(n-1), \quad n = 1, 2, \ldots. \tag{A 6}$$

The starting value $U(0)$ is given from Fresnel integrals (Abramowitz & Stegun 1964):

$$U(0) = (2\pi)^{\frac{1}{2}}[\tfrac{1}{2}(1+\mathrm{i}) - C_2(y_0) - \mathrm{i}S_2(y_0)]. \tag{A 7}$$

The recurrence formula (A 6) is stable in the forward direction. Since $U(n)$ decreases rapidly with n, to avoid underflow cancellation in computations, it is convenient to define $\bar{U}(n) \equiv \Gamma(n+\frac{1}{2})U(n)$, which has the neutrally stable forward recurrence formula

$$\bar{U}(n) = \Gamma(n-\tfrac{1}{2})\,\mathrm{e}^{\mathrm{i}y_0}\,y_0^{\frac{1}{2}-n} + \mathrm{i}\bar{U}(n-1), \quad n = 1, 2, \ldots, \tag{A 8}$$

with the starting value $\bar{U}(0) = \pi^{\frac{1}{2}}U(0)$. The use of $\bar{U}$ in (A 4) is numerically more robust and preferred. In practice, the summations in (A 4) are truncated for a prescribed equal-ripple tolerance according to the magnitudes of the original

l	m	n	Eq. (A 4)	Romberg quadrature
1	2	3	(0.001886, 0.003742)	(0.001886, 0.003742)
5	3	6	(−0.006758, 0.002120)	(−0.006758, 0.002120)
9	9	12	(−0.011812, −0.034072)	(−0.011812, −0.034072)
11	11	14	(0.109891, 0.000471)	(0.109891, 0.000471)
14	9	17	(−0.361132, 0.022987)	(−0.361132, 0.022987)
12	12	15	(−0.040432, −0.246567)	(−0.040433, −0.246565)
13	13	17	(−0.240835, 0.712153)	(−0.240853, 0.712166)

TABLE 5. Numerical verification of (A 4) for evaluating the integral of triple products of Hankel functions, (A 1). The difference $I^1_{lmn}(x_2)$-$I^1_{lmn}(x_1)$ obtained from two evaluations of (A 4) and from direct Romberg quadrature (tolerance 10^{-6}) over the interval (x_1, x_2) are compared for $x_1 = 10$, $x_2 = 11$, and $\alpha = 4$.

Chebyshev coefficients. The other integrals in (2.42) are evaluated in a similar manner.

To give an indication of the accuracy of the present method, we calculate (A 1) for two partition points x_1, x_2 according to (A 4), and compare their difference to that computed by numerical Romberg quadrature over (x_1, x_2). The results for a range of orders l, m, n are given in table 5. The accuracy is satisfactory but diminishes somewhat with increasing orders due to round-off cancellations associated with the slow convergence of (A 4).

Appendix B: Expressions for the second-order forces and moments on a bottom-extended vertical cylinder

The solution for the second-order horizontal force on a bottom-seated vertical cylinder has been studied by Molin & Marion (1986) and Eatock Taylor & Hung (1987). We extend the results to the second-order overturning moment also. The first-order total potential is

$$\phi^{(1)} = \frac{-igA}{\omega}\frac{\cosh k(z+h)}{\cosh kh}\sum_{n=0}^{\infty}\epsilon_n \mathrm{i}^n\left[J_n(k\rho) - \frac{J'_n(ka)}{H'_n(ka)}H_n(k\rho)\right]\cos n\theta, \tag{B 1}$$

and the first-order forces and moments are given in closed form.

From (3.4) and (3.6), the component of the second-order mean and double-frequency horizontal force and overturning moment (about the centre of the cylinder bottom) due to quadratic products of the first-order potential can be evaluated:

$$\frac{F^{(2)}_{x1}}{\rho_0 gaA^2} = \frac{2\mathrm{i}}{\pi(ka)^2}\sum_{n=0}^{\infty}\frac{(-1)^n}{H'_n(ka)\,H'_{n+1}(ka)}\left[3 - \frac{2kh}{\sinh 2kh} + \frac{n(n+1)}{(ka)^2}\left(1 + \frac{2kh}{\sinh 2kh}\right)\right], \tag{B 2}$$

$$\frac{M^{(2)}_{y1}}{\rho_0 gahA^2} = \frac{4\mathrm{i}}{\pi(ka)^2}\sum_{n=0}^{\infty}\frac{(-1)^n}{H'_n(ka)\,H'_{n+1}(ka)}\left\{1 + \frac{2kh}{\sinh 2kh}\left[\left(\frac{n(n+1)}{(ka)^2}+1\right)Z(kh) - \tfrac{1}{2}\right]\right\}, \tag{B 3}$$

$$\frac{\bar{F}^{(2)}_{x}}{\rho_0 gaA^2} = \frac{4}{\pi^2(ka)^3}\left(1 + \frac{2kh}{\sinh 2kh}\right)\sum_{n=0}^{\infty}\frac{[1 - n(n+1)/(ka)^2]^2}{[J'^2_n(ka) + Y'^2_n(ka)]\,[J'^2_{n+1}(ka) + Y'^2_{n+1}(ka)]}, \tag{B 4}$$

$$\frac{\bar{M}^{(2)}_{y}}{\rho_0 gahA^2} = \mathrm{Re}\left\{\frac{-4\mathrm{i}}{\pi(ka)^2}\sum_{n=0}^{\infty}\frac{1}{H'_n(ka)\,H'^{*}_{n+1}(ka)}\left[-1 + \frac{2kh}{\sinh 2kh}\left(\left(\frac{n(n+1)}{(ka)^2}+1\right)Z(kh) - \tfrac{1}{2}\right)\right]\right\}, \tag{B 5}$$

where $Z(kh) \equiv \frac{1}{4} + (2kh \sinh 2kh - \cosh 2kh + 1)/8(kh)^2$,

and the Wronskian $J_n(ka)H'_n(ka) - J'_n(ka)H_n(ka) = 2\mathrm{i}/\pi ka$

is used.

From (3.5), the second-order potential forces and moments ($F_2^{(2)}$) have components that depend on the second-order incident wave $\phi_{\mathrm{I}}^{(2)}$ ($F_{2\mathrm{I}}^{(2)}$) and diffracted wave $\phi_{\mathrm{D}}^{(2)}$ ($F_{2\mathrm{D}}^{(2)}$) respectively. Expanding the incident wave potential (2.3*b*) into partial waves, the Froude–Krylov components can be readily calculated:

$$\frac{F_{x2\mathrm{I}}^{(2)}}{\rho_0 g a A^2} = \frac{-3\mathrm{i}\pi J_1(2ka)}{2\sinh^2 kh}, \tag{B 6}$$

$$\frac{M_{y2\mathrm{I}}^{(2)}}{\rho_0 g a h A^2} = \frac{-3\mathrm{i}\pi \tanh kh}{2\sinh^4 kh} J_1(2ka)\left[\frac{\sinh 2kh}{2} - \frac{\cosh 2kh - 1}{4kh}\right]. \tag{B 7}$$

The diffraction component can be obtained via (3.14) in terms of assisting radiation potentials for horizontal translation (ψ_1) and pitch rotation (with respect to the bottom) (ψ_5). These potentials are given by

$$\begin{bmatrix}\psi_1\\ \psi_5\end{bmatrix} = \cos\theta\left\{\begin{bmatrix}\Lambda_{10}\\ \Lambda_{50}\end{bmatrix}\frac{\cosh k_2(z+h)}{k_2}\frac{H_1(k_2\rho)}{H'_1(k_2 a)} + \sum_{m=1}^{\infty}\begin{bmatrix}\Lambda_{1m}\\ \Lambda_{5m}\end{bmatrix}\frac{\cos\kappa_{2m}(z+h)}{\kappa_{2m}}\frac{K_1(\kappa_{2m}\rho)}{K'_1(\kappa_{2m}a)}\right\}. \tag{B 8}$$

The coefficients Λ_1, Λ_5 are obtained by integrating the vertical eigenfunctions with 1 and $(z+h)$ respectively in z:

$$\left.\begin{aligned}\Lambda_{1m} &= \frac{4\sinh k_{2m}h}{2k_{2m}h + \sinh 2k_{2m}h},\\ \Lambda_{5m} &= \frac{4(k_{2m}h\sinh k_{2m}h - \cosh k_{2m}h + 1)}{k_{2m}(2k_{2m}h + \sinh 2k_{2m}h)},\end{aligned}\right\} \quad m = 0, 1, 2, \ldots, \tag{B 9}$$

where $k_{20} \equiv k_2$, $k_{2m} \equiv \mathrm{i}\kappa_{2m}$, $m = 1, 2, \ldots$, and κ_{2m} are the real roots of (2.32) with ω replaced by 2ω.

From (3.14), the diffraction components are given by

$$\begin{bmatrix}F_{x2\mathrm{D}}^{(2)}\\ M_{y2\mathrm{D}}^{(2)}\end{bmatrix} = \begin{bmatrix}F_{x2\mathrm{H}}^{(2)} + F_{x2\mathrm{P}}^{(2)}\\ M_{y2\mathrm{H}}^{(2)} + M_{y2\mathrm{P}}^{(2)}\end{bmatrix} = 2\mathrm{i}\rho_0\omega a\int_{-h}^{0}\mathrm{d}z\int_0^{2\pi}\mathrm{d}\theta\begin{bmatrix}\psi_1\\ \psi_5\end{bmatrix}\frac{\partial\phi_{\mathrm{I}}^{(2)}}{\partial\rho} + \frac{2\mathrm{i}\rho_0\omega}{g}\int_0^{2\pi}\mathrm{d}\theta\int_a^{\infty}\rho\,\mathrm{d}\rho\, q\begin{bmatrix}\psi_1\\ \psi_5\end{bmatrix}_{z=0}. \tag{B 10}$$

Using (B 8), the first term can be integrated to yield

$$\begin{bmatrix}F_{x2\mathrm{H}}^{(2)}/\rho_0 g a A^2\\ M_{y2\mathrm{H}}^{(2)}/\rho_0 g a h A^2\end{bmatrix} = \frac{3\pi\mathrm{i}k^2\tanh khJ'_1(2ka)}{\sinh^4 kh}\left\{\begin{bmatrix}\Lambda_{10}\\ \Lambda_{50}\end{bmatrix}\frac{\Pi_0 H_1(k_2 a)}{k_2 H'_1(k_2 a)} + \sum_{m=1}^{\infty}\begin{bmatrix}\Lambda_{1m}\\ \Lambda_{5m}\end{bmatrix}\frac{\Pi_m K_1(\kappa_{2m}a)}{\kappa_{2m}K'_1(\kappa_{2m}a)}\right\}, \tag{B 11}$$

where $$\Pi_m = \frac{1}{2}\left[\frac{\sinh(2k + k_{2m})h}{2k + k_{2m}} + \frac{\sinh(2k - k_{2m})h}{2k - k_{2m}}\right], \quad m = 0, 1, 2, \ldots. \tag{B 12}$$

The second term of (B 10) represents the contribution due to ϕ_{P} and is simplified somewhat after integration in θ:

$$\begin{bmatrix}F_{x2\mathrm{P}}^{(2)}/\rho_0 g a A^2\\ M_{y2\mathrm{P}}^{(2)}/\rho_0 g a h A^2\end{bmatrix} = 8\pi\mathrm{i}\int_{ka}^{\infty}\mathrm{d}(k\rho)\, k\rho\bar{q}_1\begin{bmatrix}\psi_1/a\\ \psi_5/ah\end{bmatrix}_{z=0,\,\theta=0}, \tag{B 13}$$

where

$$\bar{q}_1 = \sum_{n=0}^{\infty} (-1)^n \Big\{ Y'_n(k\rho)\, Y'_{n+1}(k\rho) - J'_n(k\rho)\, J'_{n+1}(k\rho). \\ + [Y_n(k\rho)\, Y_{n+1}(k\rho) - J_n(k\rho)\, J_{n+1}(k\rho)] \left[\frac{n(n+1)}{(k\rho)^2} - \tfrac{1}{2} + \tfrac{3}{2} \tanh^2 kh \right] \Big\}, \quad \text{(B 14)}$$

and $Y_n(k\rho) \equiv J_n(k\rho) - (J'_n(ka)/H'_n(ka)) H_n(k\rho)$. The free-surface integral in (B 13) can be elevated as described in §2.4.

REFERENCES

Abramovitz, M. & Stegun, I. A. 1964 *Handbook of Mathematical Functions.* Washington: Government Printing Office.

Black, J. L. 1975 Wave forces on vertical axisymmetric bodies. *J. Fluid Mech.* **67**, 369–376.

Chakrabarti, S. K. 1978 Comments on second-order wave effects on a large diameter vertical cylinder. *J. Ship Res.* **22**, 266–268.

Chen, M. C. & Hudspeth, R. T. 1982 Nonlinear diffraction by eigenfunction expansions. *J. Waterways Port Coastal & Ocean Div. ASCE* **108**, 306–325.

Eatock Taylor, R. & Hung, S. M. 1987 Second order diffraction forces on a vertical cylinder in regular waves. *Appl. Ocean Res.* **9**, 19–30.

Faltinsen, O. M. & Löken, A. E. 1978 Drift forces and slowly-varying horizontal forces on a ship in waves. *Proc. Symp. Applied Maths, Univ. Tech. Delft.*

Fenton, J. G. 1978 Wave forces on vertical bodies of revolution. *J. Fluid Mech.* **85**, 241–255.

Fernandes, A. C. 1983 Analysis of an axisymmetric pneumatic buoy by reciprocity relations and a ring source method. Ph.D. thesis, Dept. of Ocean Engineering, MIT.

Finkelstein, A. B. 1957 The initial value problem for transient water waves. *Commun. Pure Appl. Maths* **10**, 511–522.

Herfjord, K. & Nielsen, F. G. 1986 Nonlinear wave forces on a fixed vertical cylinder due to the sum frequency of waves in irregular seas. *Appl. Ocean Res.* **8**, 8–21.

Hulme, A. 1983 A ring source integral equation method for the calculation of hydrodynamic forces exerted on floating bodies of revolution. *J. Fluid Mech.* **128**, 387–412.

Hunt, J. N. & Baddour, R. E. 1981 The diffraction of nonlinear progressive waves by a vertical cylinder. *Q. J. Mech. Appl. Maths* **34**, 69–87.

Issacson, M. Q. 1977 Nonlinear wave forces on large offshore structures. *J. Waterways, Port, Coastal & Ocean Div. ASCE* **103**, 166–170.

John, F. 1950 On the motion of floating bodies; 2. *Commun. Pure Appl. Maths* **3**, 45–101.

Kim, M. H. & Yue, D. K. P. 1988 The nonlinear sum-frequency wave excitation and response of a tension-leg platform. *Proc. 5th Intl Conf. Behavior Offshore Structures, BOSS, Norway,* pp. 687–704.

Korsmeyer, F. T. 1988 The first- and second-order transient free-surface wave radiation problems. Ph.D. thesis, Dept. of Ocean Engineering, MIT.

Lighthill, M. J. 1979 Waves and hydrodynamic loading. *Proc. 2nd Intl Conf. Behavior Offshore Structures, BOSS, London,* pp. 1–40.

Löken, A. E. 1986 Three dimensional second order hydrodynamic effects on ocean structures in waves. *University of Tronheim. Dept. of Marine Technology. Rep.* UR-86-54.

Luke Y. L. 1975 *The Special Functions and their Approximations.* Academic.

Mei, C. C. 1978 Numerical methods in water-wave diffraction and radiation. *Ann. Rev. Fluid Mech.* **10**, 393–416.

Molin, B. 1979 Second order diffraction loads upon three dimensional bodies. *Appl. Ocean Res.* **1**, 197–202.

Molin B. & Marion, A. 1986 Second order loads and motions for floating bodies in regular waves. *Proc. Offshore Mechanics & Arctic Engineering, OMAE, Tokyo,* vol. 1, pp. 353–360.

NEWMAN, J. N. 1967 The drift force and moment on ships in waves. *J. Ship Res.* **11**, 51–60.

NEWMAN, J. N. 1985 Algorithms for the free surface Green function. *J. Engng Maths* **19**, 57–67.

OGILVIE, T. F. 1983 Second order hydrodynamic effects on ocean platforms. *Intl Workshop Ship & Platform Motion, Berkeley*, pp. 205–265.

PETERS, A. S. & STOKER, J. J. 1957 The motion of a ship, as a floating rigid body, in a seaway. *Commun. Pure Appl. Maths* **10**, 399–490.

PETRAUSKAS, C. & LIU, S. V. 1987 Springing force response of a tension leg platform. *Offshore Technology Conf.*, OTC, Houston, no. 5458.

RAHMAN, M. 1983 Wave diffraction by large offshore structures; an exact second order theory. *Appl. Ocean Res.* **6**, 90–100.

SARPKAYA, T. & ISAACSON, M. 1981 *Mechanics of Wave Forces on Offshore Structures*. Van Nostrand Reinhold.

STOKER, J. J. 1957 *Water Waves*. Interscience.

WANG, P. F. 1987 The radiation condition and numerical aspects of second order surface wave radiation and diffraction. Ph.D. thesis, Dept. of Ocean Engineering, MIT.

WEHAUSEN, J. V. 1980 Perturbation methods in diffraction. *J. Waterways Port Coastal & Ocean Div. ASCE* **106**, 290–291.